Technical University of Liberec
Department of Physics, Faculty of Education

and

ICPR
International Center for Piezoelectric Research

DOMAIN ENGINEERING IN FERROELECTRIC MATERIALS

Jiří Erhart

THESIS FOR HABILITATION

Liberec **May, 2001**

Acknowledgement

This work has been created during sabbatical semester granted by the Faculty of Education, Technical University of Liberec and has been sponsored by the Ministry of Education of the Czech Republic by the grant No. J11/98242200002.

This work has been partly supported also by DARPA (Defense Advanced Research Project Administration) under the grant project No.6518 (Single Crystal Physics on PZN-PT and PMN-PT crystals) provided by Crystal Associates, Inc., East Hanover, New Jersey, U.S.A.

Scanning force microscopy experiments were done in collaboration with Prof.P.Günter and M.Abplanalp from the Nonlinear Optics Laboratory, Institute of Quantum Electronics, ETH Hőnggerberg, Zürich, Switzerland and were cosponsored also by Swiss National Science Foundation.

Theoretical investigations of the effective symmetry and material properties of twinned ferroelectric crystals were realized during my stay with the Materials Research Laboratory, Pennsylvania State University, University Park, U.S.A. under the supervision of Prof.Wenwu Cao.

Author would like to acknowledge a support and stimulating discussions on domain phenomena in ferroelectrics from Prof.Jan Fousek from the Department of Physics, Technical University of Liberec. Support from other colleagues (namely from D.Barošová and M.Šulc) from the Department of Physics and from the Department of Electronics and Electromechanical Systems (J.Nosek), Technical University of Liberec is also appreciated.

Last but not least, support from my wife Vladimíra Erhartová and from my family during writing this manuscript was substantial and is highly acknowledged.

Jiří Erhart

Contents

Introduction 1

1. Domain engineering in ferroelectric crystals 3
1.1 Present state of problem 3
1.2 Domain structure observations 4
1.3 Measurement of material properties 5
1.4 Theory 7
1.5 Applications 7

2. Effective symmetry and material properties of twin-domain ferroelectric crystal 11
2.1 Microscopic and macroscopic symmetries 11
2.2 Effective material properties of twinned single-crystal containing only one set of twins 13
2.3 Conclusions 15

3. Domain structure observations in PZN-PT and PMN-PT crystals 27
3.1 Experimental method 27
3.2 Results and discussion 28
3.2.1 (001) oriented samples 29
3.2.2 (110) oriented samples 30
3.2.3 Local hysteresis curves 31
3.3 Conclusions 32

4. Future perspectives of domain engineering in ferroelectric crystals 44
4.1 Ferroelectric species $m\bar{3}m \rightarrow 4mm$ 45
4.2 Ferroelectric species $m\bar{3}m \rightarrow mm2$ 45
4.3 Ferroelectric species $4/mmm \rightarrow m_{y}$ 46
4.4 Ferroelectric species $4/mmm \rightarrow mm2$ 47
4.5 Ferroelectric species $\bar{4}3m \rightarrow m_{xy} m_{\bar{x}y} 2_{z}$ 47
4.6 Ferroelectric species $\bar{4}3m \rightarrow 3_{xyz} m_{\bar{x}y}$ 47
4.7 Ferroelectric species $3m \rightarrow 1$ 48
4.8 Conclusions 48

Conclusions 49
Appendix I 50
Bibliography 60

Introduction

Ferroelectrics (as well as other ferroic materials like ferroelastics, etc.) play an essential role in a number of technical applications. In some of them, dynamic processes are essential (like ferroelectric memories subjected to the numerous switching processes), in others the static domain distribution is crucial for material properties. In presented work, we concentrate mostly on the static domain configurations.

Domain-engineered crystal structures were recently [1] classified into two principally different cases:

- Domain-geometry-engineered structures
- Domain-average-engineered structures.

First group belongs to the applications where the exact spatial distribution of domains is essential for material function. Possible applications of such domain-engineered crystals cover non-linear optical devices, e.g. devices for second harmonic generation. Well-defined domain regions and their spatial arrangement are important. Example of such material is periodically poled $LiNbO_3$ crystal.

Second group of domain-engineered crystals exhibit extremely large material properties, like piezoelectric coefficients, with respect to the single-domain crystal. Despite of a great effort invested in research of such single-crystals in last decade, an origin of superior piezoelectric coefficients is not known up to now. Examples of these materials could serve solid solutions of PZN-PT and PMN-PT.

Superior piezoelectric material properties have been created in multi-domain PZN-PT and PMN-PT single-crystals. It is supposed to get further improvement of desired material properties owing to the domain-engineered crystal structure. Such idea is very much similar to the idea of non-homogeneous piezoelectric composite materials, which are widely studied for many years [2,3]. In general, domain engineering ***is not possible*** in ceramic materials due to the random grain orientations.

Beginning by the discovery of possible material property enhancement (e.g. piezoelectric coefficient enhancement in PZN-9%PT [4]), material properties are no more fully described just by the material chemical composition. Domain structure, which plays an essential role in material properties, must be also specified to describe fully particular material state. Up to the discovery of domain engineering, single-domain crystal was supposed to be the best possibility for any application. This situation is also reflected by IEEE Std. 176-1987 (Standard on Piezoelectricity), which recommends resonant measurement methods suitable mostly for single-domain crystals. While the domain-engineered crystal structure is not fully reproducible sample by sample, resonant measurement methods should be modified in order to get as much as possible material coefficients on the same crystal sample, i.e. on the sample with the same domain structure.

Domain engineering studies have been mostly reported for solid solutions of PZN-PT and PMN-PT. Some attempts have been also done on pure PZN and $BaTiO_3$ crystals. All these materials belong to perovskite relaxor or normal ferroelectrics. The biggest piezoelectric coefficient enhancement ever has been measured in PZN-PT and PMN-PT solid solutions for certain chemical compositions with crystallographic rhombohedral symmetry (*3m*). Some domain-engineered crystal structures have been studied in tetragonal (*4mm*), orthorhombic (*mm2*) and rhombohedral (*3m*) $BaTiO_3$.

First chapter of this work is devoted to the description of material and crystallographic (ferroelectric species) nature of structural ferroelectric phase transitions in PZN, PZN-PT, PMN-PT and $BaTiO_3$ crystals. Literature on major domain and

domain wall phenomena is reviewed. Major theoretical and experimental achievements in the research of domain-engineered crystal structures on PZN-PT, PMN-PT and $BaTiO_3$ are discussed in details.

Second chapter focuses on our own theoretical analysis [36,37] of the effective symmetry and the effective material properties in twinned ferroelectric crystals belonging to the tetragonal $m\bar{3}m \rightarrow 4mm$, rhombohedral $m\bar{3}m \rightarrow 3m$ and orthorhombic $m\bar{3}m \rightarrow mm2$ ferroelectric species. Based on the knowledge of the single-domain material properties and the domain volume ratio presented method allows for calculation of the effective material properties.

The objective of the third chapter of this work is our own work [43,44] done on domain engineered crystals. Domain structure observations by piezoresponse mode Scanning Force Microscopy (SFM) are discussed in details in PZN-8%PT and PMN-29%PT crystals. SFM technique is further compared with optical observations made on the crystals by polarizing microscopy.

Fourth chapter deals with future perspectives in domain engineering of other ferroelectric materials with more than two permissible domain states which were not reported previously. Domain wall structures and possible promissing directions for poling electric field in several ferroelectric species are discussed.

Short conclusion summarizes major achievements as well as future perspectives in domain engineering on ferroelectric crystals.

1. Domain engineering in ferroelectric crystals

This chapter is focused on the major results reported for domain-engineered crystal structures in PZN, PZN-PT, PMN-PT and $BaTiO_3$ (BT) crystals. These crystals are the only ones where the domain-average-engineering was studied and reported in the literature. Domain-geometry-engineering is not reviewed here however also e.g. periodically poled domain structures are extensively studied for nonlinear optical applications.

1.1 Present state of the problem

Solid solutions of $Pb(Mg_{1/3}Nb_{2/3})O_3 - PbTiO_3$ (PMN-PT) and $Pb(Zn_{1/3}Nb_{2/3})O_3 - PbTiO_3$ (PZN-PT) are the first crystal systems with multi-domain engineered structure which improves significantly their piezoelectric response. Moreover, these two systems exhibit such piezoelectric properties [4-6] in the temperature range important for applications. It makes these systems very attractive for further study as well as for the applications. It is suggested that the multi-domain structure fundamentally present in the crystal is an origin of such material behavior, although the exact mechanism is not known up to now. Domain structure, its equilibrium structure, spatial distribution and dynamics are of fundamental importance for such systems.

Single crystals of solid solutions between ferroelectric perovskites PZN or PMN and $PbTiO_3$ (PT) has been grown over the wide compositional range starting 40 years ago. The solid solution between ferroelectric PZN (PMN) with rhombohedral symmetry ($m\bar{3}m \rightarrow 3m$) and PT with tetragonal symmetry ($m\bar{3}m \rightarrow 4mm$) has naturally a morphotropic phase boundary (MPB) – for phase diagram see Fig.1. MPB cover a range of 8-10% molar PT content in PZN-PT [6] and 33-35% molar PT content in PMN-PT [7] at room temperature. Extremely high piezoelectric and dielectric properties [4,8-9] appear for chemical compositions near MPB in rhombohedral phase. Moreover the values of the piezoelectric constants and the electromechanical coupling factors so far reported are significantly higher than those one in PZT ceramics [23]. Such huge piezoelectric properties are very welcome in designing e.g. the probes for medical ultrasound equipment or sonars for military use.

Although the PZN-PT (PMN-PT) system is known for many years, only recently the improvement in growing significantly larger single-crystals made possible further progress especially in resonant measurements of the piezoelectric properties. Also the idea of domain-engineered samples, rather than single-domain crystals, seems to be very promissing in getting desired physical properties.

The MPB in the PZN-PT (PMN-PT) phase diagram is the phase boundary between rhombohedral and tetragonal solid solutions. Common higher temperature phase (parent phase) is a cubic, i.e. non-ferroelectric (also non-piezoelectric) phase. Solid solutions for rhombohedral compositions have 8 possible domain states (Fig. 2) with the spontaneous polarization oriented in one of the directions of {111}-family. For the tetragonal compositions there are 6 domain states, with the spontaneous polarization oriented along one of the directions of {100}-family.

Crystals are grown by high-temperature flux method using excess PbO as a flux [10,11]. Grown single crystals are of irregular shape and light-brown opalesque color. If heated above the transition temperature (i.e. Curie temperature) to cubic phase, they are transparent. Grown crystals are removed from the mixture by the hot nitric acid, then cut, polished, electroded and poled. Typical size of crystals is 3-20mm, sometimes even larger in some crystallographic directions.

Poling of PZN-PT (PMN-PT) single-crystals could be done by two different methods. In the first procedure, the single crystals are poled at room temperature by applying electric field of *4kV/mm*. Another poling procedure is so called "field-freezing" from the temperature above Curie temperature (phase transition to the paraelectric phase) by applying electric field *1kV/mm* [8]. Curie temperature is relatively low (about $200^{o}C$) and dependent on the chemical composition. Electric field during poling process is applied or in [100]-direction for tetragonal compositions, or in [111]-direction for rhombohedral compositions in attempt to get single-domain crystal. If the poling field is applied along [100]-direction for the rhombohedral phase (i.e. in the direction ***different*** from all possible spontaneous polarization directions), the resulting crystal has complicated multi-domain structure. Surprisingly, the crystals poled by applying electric field of such direction exhibit significantly higher piezoelectric coefficients.

1.2 Domain structure observations in domain-engineered crystals

Extensive attention has been paid to the observation of the domain structure under various conditions (temperature, electric field) [12-20]. Domain switching and its dynamic are observed and reported.

Domain structure corresponds to the tetragonal and rhombohedral symmetry for PZN-PT (PMN-PT) single-crystals for certain chemical compositions and poled along one of the directions of the spontaneous polarization (i.e. {100} in tetragonal, or {111} in rhombohedral phase). For rhombohedral PZN-PT crystal poled along [001]-direction, complicated multi-domain structure is observed. Such domain structure is very stable under electric field contrary to the crystal poled in [111]-direction. In [001]-poled crystal, only the density of domain walls changes when the electric field is applied. No changes in domain wall morphology are observed by the optical microscopy. In [111]-poled crystals not only the density of domain walls but also the morphology changes. Electric field applied in [111]-direction causes the domain wall movements. This behavior suggests easier domain switching in [001]-poled rhombohedral crystals due to the stable domain wall structure and as a consequence also the hysteresis-free strain vs. electric field behavior is observed [8,9]. On the contrary, in [111]-poled rhombohedral crystals complete re-configuration of domain walls is taking place during electric switching and hysteretic behavior is observed in elastic strain induced by the electric field.

Domain structure of PZN-PT and PMN-PT single-crystals with chemical compositions near the MPB is reported as a complicated mixture of both (rhombohedral and tetragonal) phases. It seems that the tetragonal phase domains [17] can coexist with the rhombohedral one also in rhombohedral phase near MPB. No similar coexistence of rhombohedral and tetragonal phase domains in tetragonal phase near MPB has been reported.

Environmental Scanning Electron Microscopy (ESEM) technique has been used to study etched surface of PZN-PT single-crystals [24]. Dendritic domain structures were found at the surface of PZN-4.5%PT (rhombohedral phase far from MPB), PZN-8%PT (rhombohedral phase near to MPB) and PZN-12%PT (tetragonal phase). Density of dendrite structures changes after poling. It is anticipated that the structure observed is due to the ferroelectric domains created as a result of the crystal defects and space charges. Domain walls are of random orientation not corresponding to the equilibrium orientations of domain walls for ferroelectric species involved. Typical size of dendritic structures is about 10-100μm.

Domain structure is also reported for pure PZN crystals (rhombohedral $m\bar{3}m \rightarrow 3m$ phase) poled either in [111]- or [001]-direction [21,22]. In some of the crystal parts domains correspond to the crystallographic orientations in rhombohedral ferroelectric phase, in other portions non-crystallographic ferroelastic domain wall orientations were observed. It is supposed to be due to the internal crystal defects. Defects can generate weak local stress fields and they account for polar micro region ordering.

Domain structure has been also observed in [111]-poled BT at room temperature under different electric field conditions [25]. Orthorhombic as well as rhombohedral phase induced from tetragonal phase by an electric field was observed by optical microscopy at certain level of the electric field.

1.3 Measurement of material properties of domain-engineered crystals

Single-crystal of PZN-8%PT exhibited piezoelectric coefficient d_{33}~*2000pC/N* and electromechanical coupling coefficient k_{33}~*90%*, if poled in [001]-direction [8,9,20]. This direction is not a direction of any of the permissible spontaneous polarization in rhombohedral phase. Such single-crystal could not be in a single-domain state, in general. Such piezoelectric material property is the biggest ever observed in any of the materials in the range of the technically important temperatures. Piezoelectric coefficient is 4-5 times larger than for the usually used PZT ceramics [23]. Extremely high values of the electric field induced strain without significant hysteresis have been reached in PZN-PT domain-engineered structure.

Wide variety of material properties measured by various methods has been already reported for PZN-PT and PMN-PT system [4,7-9,20,26-27]. Resonant as well as ultrasound techniques are reported. Although such extensive effort has been done, complete set of the elastic, piezoelectric and dielectric properties has been published only for PZN-4.5%PT poled along [001]-direction [26] (Table 1.1). Up to now, no complete set of the material properties has been reported for the tetragonal phase and for the compositions near the MPB in rhombohedral phase for domain-engineered PZN-PT single-crystals. Also, the published measurement results do not take into account the actual domain structure in particular sample used for the measurement. Results of such measurements are not reproducible for other samples. All measurements reported were done under the assumption of the tetragonal effective symmetry for the rhombohedral [001]-poled domain-engineered samples. No basic crystallographic (rhombohedral or tetragonal) single-domain material properties have been reported yet.

Table 1.1 – Material properties of [001]-poled PZN-4.5%PT single-crystal [26]

Elastic moduli $c_{ij}[10^{10}N/m^2]$											
c^E_{11}	c^E_{12}	c^E_{13}	c^E_{33}	c^E_{44}	c^E_{66}	c^D_{11}	c^D_{12}	c^D_{13}	c^D_{33}	c^D_{44}	c^D_{66}
11.1	10.2	10.1	10.5	6.4	6.3	11.3	10.4	9.5	13.5	6.7	6.3
Elastic constants $s_{ij}[10^{-12}m^2/N]$											
s^E_{11}	s^E_{12}	s^E_{13}	s^E_{33}	s^E_{44}	s^E_{66}	s^D_{11}	s^D_{12}	s^D_{13}	s^D_{33}	s^D_{44}	s^D_{66}
82.0	-28.5	-51.0	108	15.6	15.9	61.5	-49.0	-9.0	20.6	14.9	15.9
Piezoelectric coefficients $e[C/m^2]$, $d[10^{-12}C/N]$, $g[10^{-3}Vm/N]$, $h[10^8V/m]$											
e_{15}	e_{31}	e_{33}	d_{15}	d_{31}	d_{33}	g_{15}	g_{31}	g_{33}	h_{15}	h_{31}	h_{33}
8.9	-3.7	15.0	140	-970	2000	5.0	-21.0	44	3.4	-4.3	17
Dielectric constant $\varepsilon[\varepsilon_0]$, $\beta[10^{-4}/\varepsilon_0]$								Electromechanical coupling coefficients			
ε^S_{11}	ε^S_{33}	ε^T_{11}	ε^T_{33}	β^S_{11}	β^S_{33}	β^T_{11}	β^T_{11}	k_{15}	k_{31}	k_{33}	k_t
3000	1000	3100	5200	3.4	10.0	3.2	1.9	0.23	0.50	0.91	0.50

Material properties like d_{33}, k_{33}, d_{31} exhibit extremely high values in [001]-poled PZN-PT or PMN-PT in rhombohedral phase near the MPB. Also the measurements of the hydrostatic piezoelectric coefficient d_h [4], spontaneous polarization $\boldsymbol{P}_S$ [5] and electrostrictive properties [28] have been previously reported. It is relatively rare to find references for the measurement of the temperature dependence of any of the material property. Temperature dependence of k_{33} and d_{33} as well as ε_{33} and $\boldsymbol{P}_S$ were reported for PZN-9%PT [29].

Ferroelectric fatigue [30] has been studied in PZN-PT single crystals with various chemical compositions. Crystal of PZN-4.5%PT exhibits rhombohedral phase and shows low fatigue (i.e. stable values of the coercive field and the remanent polarization) up to 10^5 cycles. Hysteresis loop is very stable under electric field switching. Contrary to that [111]-poled crystal shows rapid decrease in remanent polarization and slight increase in the coercive field after 10^5 cycles. Also hysteresis loop changes significantly. Switching behavior depends also on the switching electric field strength for [111]-poled crystals and it is almost electric field amplitude independent for [001]-poled PZN-4.5%PT single crystals. [001]-poled PZN-4.5%PT single-crystals shows almost no fatigue under various field strengths up to 10^5 cycles. Similar behavior has been observed also for pure PZN crystals (rhombohedral phase).

For MPB chemical compositions (namely PZN-8%PT) crystals poled in [001]-direction remanent polarization is almost stable whereas coercive field decreases and hysteresis loop changes ("waist" of the hysteresis loop narrows). Some kind of pinning mechanism is anticipated probably due to the coexistence of rhombohedral and tetragonal phases. In tetragonal phase (namely for PZN-12%PT) crystal poled in [001]-direction significant fatigue has been observed. The above results indicate that the fatigue rate is strongly dependent on both the ferroelectric phase and the crystal orientation.

Domain switching and electromechanical properties were studied in pulse poled PZN, PZN-4.5%PT and PZN-8%PT single-crystals in both [111]- and [001]-orientations [31]. Switching current peak density is measured as a function of the field strength. Activation energy, wall mobility and critical field are calculated. In general, switching current density is measured higher in [001]- than in [111]-oriented crystals. Dendritic structures at the etched surface are observed by optical polarizing microscopy as well as by the topography Scanning Force Microscopy (SFM) technique. Typical size of the dendritic structures increases with the length of switching pulses and with the electric field strength (domain growth processes). On the contrary, density of the dendritic structures increases for shorter pulses and lower electric field (domain nucleation processes). Piezoelectric properties are calculated from the slope of the strain vs. electric field behavior at low fields. Piezoelectric d_{33} coefficient reaches values as high as *2600pC/N* at the electric field of *1kV/mm* and *1000μs* pulse.

Domain-engineered crystal system of solid solution PMN-PT has been also studied [20,32,40-42]. This crystal belongs to the same ferroelectric species like PZN-PT and exhibits similar improvement in the piezoelectric material properties due to the crystallographically domain-engineered structure. PMN-PT has rather smaller Curie temperatures than PZN-PT for corresponding chemical compositions.

Effect of uniaxial stress on the electromechanical properties has been measured in PMN-30%PT (i.e. for the chemical composition of rhombohedral phase near MPB) single-crystal and ceramics [33]. At the field level of *0.5kV/mm* slope of the strain vs. electric field curve is independent from the mechanical stress. Corresponding piezoelectric coefficient value is d_{33}*~1500pC/N* in [001]-oriented PMN-30%PT crystal.

Material properties are also reported in pure domain-engineered PZN single-crystals [8]. Improvement in the piezoelectric coefficient is also one order of magnitude, i.e. from d_{33}~*100pC/N* to d_{33}~*1100pC/N* in pure PZN crystals poled along [001]-direction.

Among the other ferroelectric materials, domain engineered domain structure has been reported recently in [001]-poled BT single-crystals in different ferroelectric phases (tetragonal *4mm*, orthorhombic *mm2* and rhombohedral *3m*) at different temperatures [34]. Unfortunately, this study was not accompanied by the domain morphology observation but only by the hysteresis loop measurement. Another attempt has been performed on [111]-poled BT at room temperature under different electric field conditions [25]. Electric field induced orthorhombic as well as rhombohedral phase were observed at certain level of the electric field applied. Enhancement in the piezoelectric material properties has been found from the hysteresis loop (strain vs. electric field) measurements. Increase in piezoelectric coefficient is from d_{33}~*100pC/N* in tetragonal phase to d_{33}~*295pC/N* in electric field induced orthorhombic phase and to d_{33}~*145pC/N* in the electric field induced rhombohedral phase.

1.4 Theory of domain-engineered crystals

Among the very rare references on the theoretical aspects of PZN-PT system, there is a calculation of the dielectric constant, phase diagram and the lattice parameters reported [35]. Based on the previously published material properties of pure PZN and PT, the phase diagram for PZN-PT solid solution is calculated. Model reported does not allow for the theoretical verification of the piezoelectric response in multi-domain crystal.

Theoretical analysis of the possible domain arrangements in domain engineered crystal has been published recently for $m\bar{3}m \rightarrow 3m$ ferroelectric species [1]. Effective symmetry of domain engineered crystal has been specified for equal volume ratio of all permissible domain arrangements. Also corresponding external fields (electric, mechanical stress) are specified for all possible multi-domain sets in order to create particular domain-engineered crystal configuration.

Effective material properties have been also calculated theoretically for twin-domain tetragonal $m\bar{3}m \rightarrow 4mm$, rhombohedral $m\bar{3}m \rightarrow 3m$ and orthorhombic $m\bar{3}m \rightarrow mm2$ crystals [36,37]. On the basis of known single-domain material properties and domain volume ratio, complete set of all effective material properties could be calculated for twin-domain system.

1.5 Applications of domain-engineered crystals

PZN-9%PT single crystals (i.e. MPB composition in rhombohedral phase) poled in [001]-direction are supposed for application as an ultrasound probes for medical diagnostics. Design of single crystal probe as well as an array of 40-channel ultrasonic probe was reported by Toshiba Corp., Japan [38,39]. Other technical application of PZN-PT and PMN-PT single-crystals (also PMN-PT ceramics) is supposed in sonars for military use, however results could not be taken from available sources. PMN-PT material is technically used in ceramic form and it is commercially available from piezoceramics manufacturers.

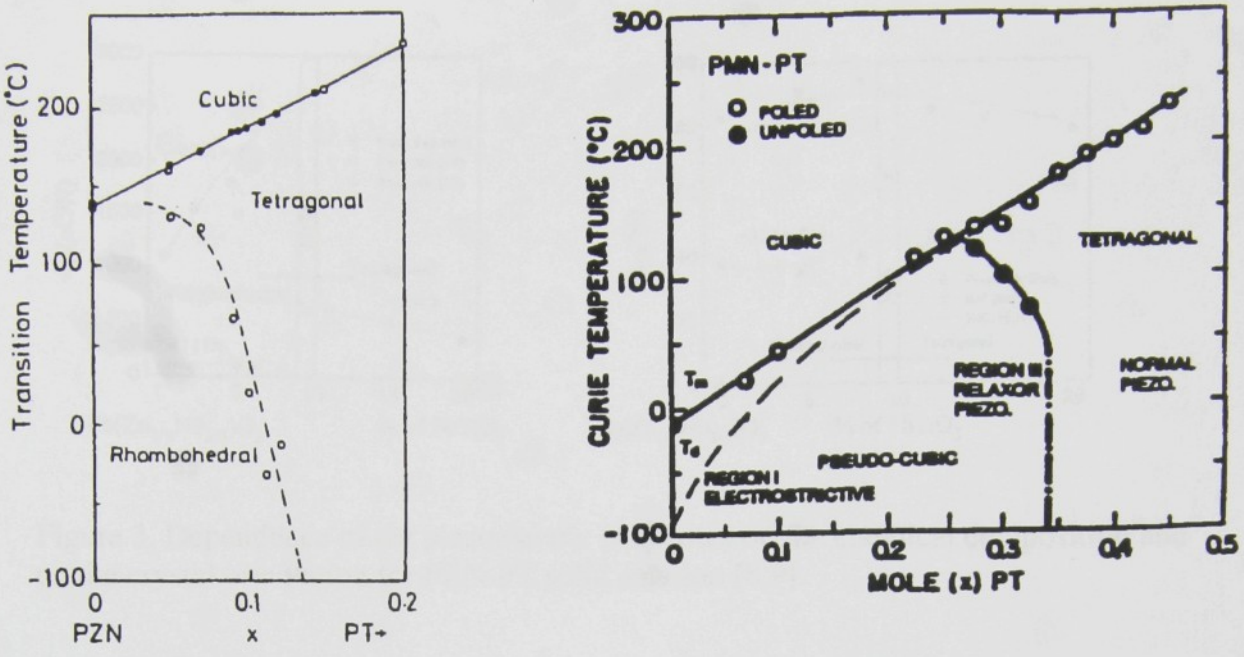

Figure 1. Phase diagram for PZN-PT [6] and PMN-PT [7] solid solutions.

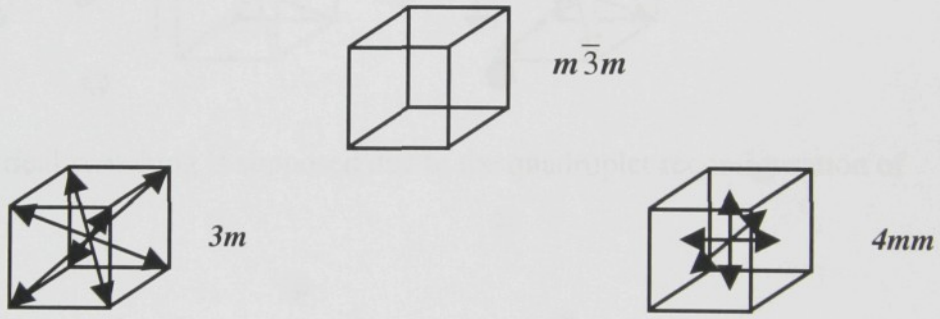

Figure 2. Permissible spontaneous polarization directions in paraelectric (cubic) and ferroelectric (tetragonal or rhombohedral) phases.

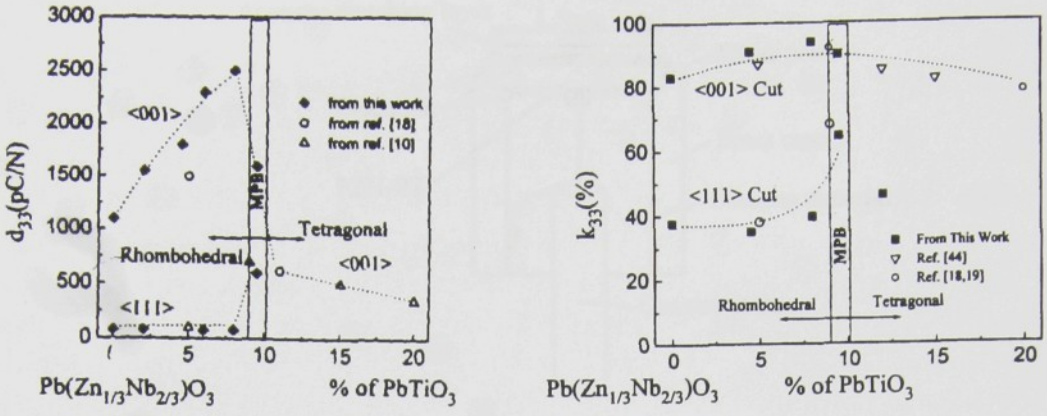

Figure 3. Dependence of the piezoelectric properties on the chemical composition and on the crystal orientation for PZN-PT solid solution [8,9].

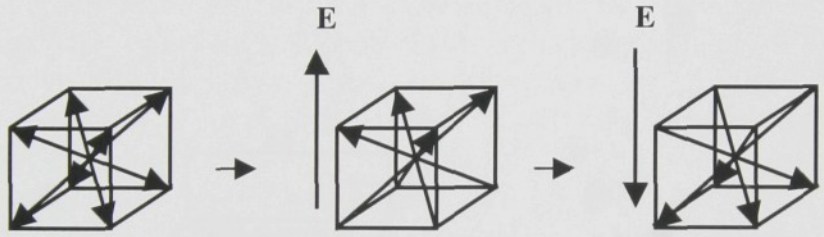

Figure 4. Electrical switching is supposed due to the quadruplet reconfiguration of domains.

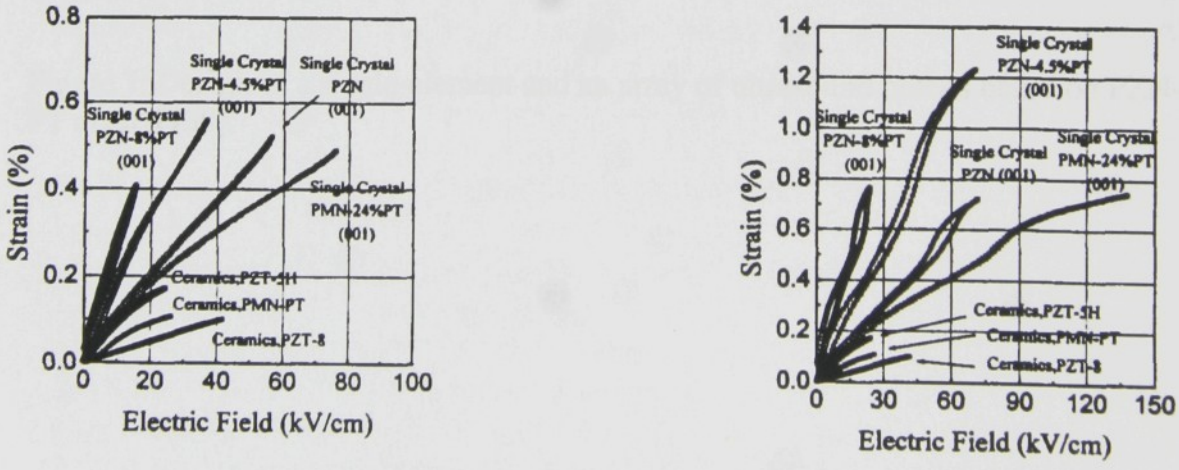

Figure 5. Comparison of the electric field-induced strain for PZN-PT, PMN-PT and PZT ceramics [8].

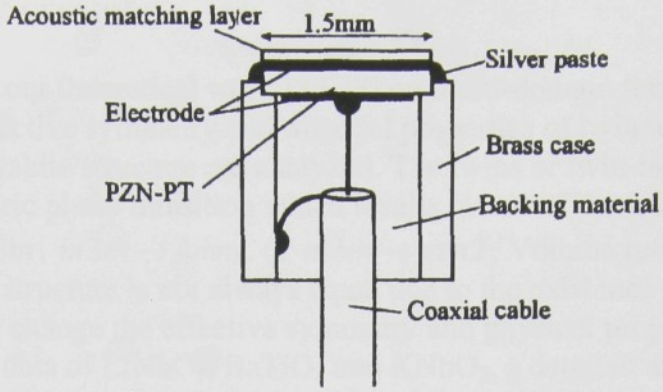

Figure 6. Design of the single ultrasound probe based on PZN-PT crystal [38].

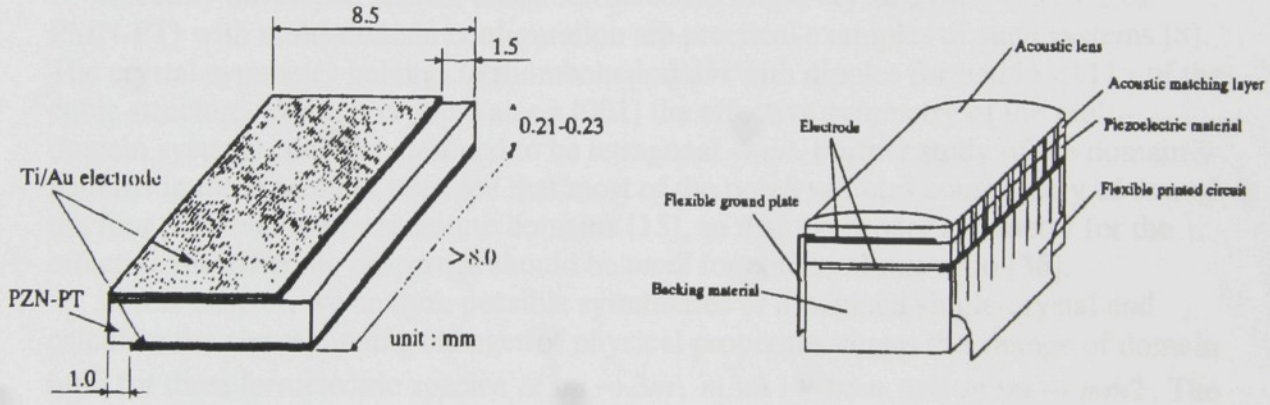

Figure 7. Design of a single-element and an array of ultrasound probes based on PZN-PT crystal [39].

2. Effective symmetry and material properties of twin-domain ferroelectric crystal

In this chapter our theoretical work [36,37] on multi-domain ferroelectric crystal is presented. The effective symmetry and material properties of twinned ferroelectric crystals with perovskite structure are analyzed. The twins or twin-bands were formed during a ferroelectric phase transition which results in one of the following symmetry changes $m\bar{3}m \rightarrow 3m$, $m\bar{3}m \rightarrow 4mm$, or $m\bar{3}m \rightarrow mm2$. Volume ratio of the two domains in a twin structure is not always equal due to the existence of defects and surfaces. This will change the effective symmetry and physical properties of the twin system. Using the data of $LiNbO_3$, $BaTiO_3$ and $KNbO_3$, a detailed analysis on material property changes caused by the deviation of equal domain volume partition was carried out.

The macroscopic properties of a multi-domain ferroelectric system are the collective contribution of many differently oriented domains. The macroscopic symmetry of a multi-domain system is different from the microscopic symmetry of the crystal. However, most applications of these twinned crystals are based on macroscopic properties, which call for a systematic analysis for twinned crystals. The symmetry refers here to the relationship between the building blocks, i.e. to the domains whose determine the macroscopic physical properties.

Recently developed relaxor based ferroelectric single-crystals (like PZN-PT or PMN-PT) with multi-domain configuration are practical examples of such systems [8]. The crystal symmetry belongs to rhombohedral *3m* with dipoles formed in <111> of the cubic structure. When it is poled along [001] the effective symmetry of the multi-domain systems could be assumed to be tetragonal *4mm*. Further study of the domain patterns in these samples revealed that most of the poled samples consist only of two of the four possible low-temperature domains [15], so that the proper symmetry for the effective macroscopic properties should be *mm2* for equal volume ratio [36].

In this chapter, we analyze possible symmetries of a twinned single-crystal and calculate the corresponding changes of physical properties versus the change of domain ratio for three ferroelectric species $m\bar{3}m \rightarrow 3m$, $m\bar{3}m \rightarrow 4mm$ and $m\bar{3}m \rightarrow mm2$. The objective is to provide the definition of effective physical properties and the associated macroscopic symmetry for twin structures, and more importantly, quantify the variation of these properties caused by the change of domain volume ratio.

2.1 Microscopic and macroscopic symmetries

In a $m\bar{3}m \rightarrow 3m$ ferroelectric phase transition, the possible directions for dipole formation are along the cube diagonals, i.e., <111> in the cubic coordinate system. In domain-engineered 95.5%PZN-4.5%PT single-crystals, the poling field was applied in [001] rather than the dipolar direction. Four domain states remain degenerate after poling with dipoles forming a 55° with the poling field. Permissible domain walls (DW's) among these ferroelectric states are listed in Table I.1 (Appendix I). Two perpendicular DW's always exist between any two given domains states, one is charged and the other is neutral. The DW orientations are illustrated in Fig.1 in the cubic coordinates.

For a charged DW of P^I and P^{II} oriented in [010] and a neutral DW of P^I and P^{III} orientation [001], the effective macroscopic symmetry of the twin structure is monoclinic *m* (Fig.1a,b). The symmetry can be raised to orthorhombic *mm2* when the

two domains have identical size (Fig.1c). The two-fold axis, which is also the direction of effective polarization, is oriented in [101] as shown in Fig.1c.

For a $m\bar{3}m \rightarrow 4mm$ ferroelectric phase transition (e.g. $BaTiO_3$), the possible spontaneous polarization directions are in <100> (in the cubic coordinate system). In domain-engineered $BaTiO_3$ single-crystals, the poling field was applied in [111] rather than the polarization directions. Three domain states remain after poling with the dipoles in each of the unit cells forming 55° with the poling field. Permissible DW's among these three remaining ferroelectric states are listed in Table I.2. (Appendix I) Similarly, two perpendicular DW's between any two given domains are permitted, one is charged and the other is neutral. The DW orientations for this case are illustrated in Fig. 2.

Again, twins containing neutral DWs and charged DWs have monoclinic *m* symmetry unless the domains are identical in size (for neutral DW the macroscopic symmetry is not higher than monoclinic *m*). Fig 2 illustrated the twin structures of P^I and P^{III} (Fig.2a) with DW oriented in (101), and twins of P^I and P^{III} (Fig.2b) with the DW oriented in $(\bar{1}01)$. For the special case of equal sized twins, the symmetry becomes *mm2* with a two-fold axis oriented in [101] direction as shown in Fig.2c. The two-fold axis is also the direction of the effective polarization of the system.

For a $m\bar{3}m \rightarrow mm2$ ferroelectric phase transition (e.g. $KNbO_3$), the possible spontaneous polarization directions are the face diagonals <110> (in the cubic coordinate system). Assuming we perform domain engineering to the sample by applying a poling field in [001], there will be four domain states (P^I, P^{II}, P^{III}, P^{IV}) remaining with permissible domain walls listed in Table I.3 (Appendix I). Possible new feature for this system is the presence of S-walls [45,46] (strange walls) which do not lie on the lattice plane and their orientation depends on the values of the elastic distortion in the two domains, therefore, changes with temperature. There are four types of S-wall orientations determined by the following relation [45]

(2.1) $S_1: \quad ds_1 + ds_2 + Kds_3 = 0$

(2.2) $S_2: \quad ds_1 - ds_2 + Kds_3 = 0$

(2.3) $S_3: \quad ds_1 - ds_2 - Kds_3 = 0$

(2.4) $S_4: \quad ds_1 + ds_2 - Kds_3 = 0$

(2.5) $$K = \frac{Q_{44}}{Q_{11} - Q_{12}}$$

where Q_{ij} are the electrostrictive coefficients in the cubic $m\bar{3}m$ phase.

DW orientations are illustrated in Fig.3. For a charged DW, such as wall between P^I and P^{III} oriented in $(\bar{1}10)$, the effective symmetry of this twin structure is triclinic with symmetry group *1* (Fig.3a). If the two domains have equal volume ratio, the symmetry is monoclinic *m* (Fig.3b). For a twin between P^{III} and P^{IV} with a charged DW oriented in (010), the effective symmetry is monoclinic *m* (Fig.3c) for unequal volume ratio and orthorhombic *mm2* when the size the two domains become the same. The two-fold axis is oriented in [001], which is also the direction of the total effective polarization (Fig.3d).

The domain states P^{III} and P^{IV} have a neutral DW oriented in (001), which again has a monoclinic symmetry *m* (Fig.3e). The S-walls are neutral in all cases as listed in Table I.3 (Appendix I). The macroscopic symmetry of a twin crystal with S-wall is always triclinic *1*.

2.2 Effective material properties of twinned single-crystal containing only one set of twins

For this case, there are only two types of domains. Using the procedure described in [36, 47], we combine the components of the elastic stress and electric field to form a vector (note: $T_4^{(i)}$ and $T_6^{(i)}$ components must be used twice)

(2.6) $\tau^{(i)} = (T_1^{(i)}, T_2^{(i)}, T_3^{(i)}, T_4^{(i)}, T_4^{(i)}, T_5^{(i)}, T_6^{(i)}, T_6^{(i)}, E_1^{(i)}, E_2^{(i)}, E_3^{(i)}), \qquad i = 1,2$

The averaging conditions can now be expressed as

(2.7) $\tau^{eff} = v^{(1)}\tau^{(1)} + v^{(2)}\tau^{(2)}$

and

(2.8) $M^{eff}\tau^{eff} = v^{(1)}M^{(1)}\tau^{(1)} + v^{(2)}M^{(2)}\tau^{(2)}$

Boundary conditions at the interfaces can be described by the compact matrix equation

(2.9) $b^{(1)}\tau^{(1)} = b^{(2)}\tau^{(2)}$

Combining Eqs. (2.6)-(2.9), the effective material properties of the twinned crystal can be expressed in the following matrix form

(2.10) $M^{eff} = [v^{(1)}M^{(1)}(b^{(1)})^{-1} + v^{(2)}M^{(2)}(b^{(2)})^{-1}][v^{(1)}(b^{(1)})^{-1} + v^{(2)}(b^{(2)})^{-1}]^{-1}$

where $v^{(1)} + v^{(2)} = 1$ are the volume ratios of the domains, matrices M and b are defined by

(2.11)
$$M^{(i)} = \begin{pmatrix}
s_{11}^{(i)} & s_{12}^{(i)} & s_{13}^{(i)} & s_{14}^{(i)} & s_{14}^{(i)} & s_{15}^{(i)} & s_{16}^{(i)} & s_{16}^{(i)} & d_{11}^{(i)} & d_{21}^{(i)} & d_{31}^{(i)} \\
s_{12}^{(i)} & s_{22}^{(i)} & s_{23}^{(i)} & s_{24}^{(i)} & s_{24}^{(i)} & s_{25}^{(i)} & s_{26}^{(i)} & s_{26}^{(i)} & d_{12}^{(i)} & d_{22}^{(i)} & d_{32}^{(i)} \\
s_{13}^{(i)} & s_{23}^{(i)} & s_{33}^{(i)} & s_{34}^{(i)} & s_{34}^{(i)} & s_{35}^{(i)} & s_{36}^{(i)} & s_{36}^{(i)} & d_{13}^{(i)} & d_{23}^{(i)} & d_{33}^{(i)} \\
s_{14}^{(i)} & s_{24}^{(i)} & s_{34}^{(i)} & s_{44}^{(i)} & s_{44}^{(i)} & s_{45}^{(i)} & s_{46}^{(i)} & s_{46}^{(i)} & d_{14}^{(i)} & d_{24}^{(i)} & d_{34}^{(i)} \\
s_{14}^{(i)} & s_{24}^{(i)} & s_{34}^{(i)} & s_{44}^{(i)} & s_{44}^{(i)} & s_{45}^{(i)} & s_{46}^{(i)} & s_{46}^{(i)} & d_{14}^{(i)} & d_{24}^{(i)} & d_{34}^{(i)} \\
s_{15}^{(i)} & s_{25}^{(i)} & s_{35}^{(i)} & s_{45}^{(i)} & s_{45}^{(i)} & s_{55}^{(i)} & s_{56}^{(i)} & s_{56}^{(i)} & d_{15}^{(i)} & d_{25}^{(i)} & d_{35}^{(i)} \\
s_{16}^{(i)} & s_{26}^{(i)} & s_{36}^{(i)} & s_{46}^{(i)} & s_{46}^{(i)} & s_{56}^{(i)} & s_{66}^{(i)} & s_{66}^{(i)} & d_{16}^{(i)} & d_{26}^{(i)} & d_{36}^{(i)} \\
s_{16}^{(i)} & s_{26}^{(i)} & s_{36}^{(i)} & s_{46}^{(i)} & s_{46}^{(i)} & s_{56}^{(i)} & s_{66}^{(i)} & s_{66}^{(i)} & d_{16}^{(i)} & d_{26}^{(i)} & d_{36}^{(i)} \\
d_{11}^{(i)} & d_{12}^{(i)} & d_{13}^{(i)} & d_{14}^{(i)} & d_{14}^{(i)} & d_{15}^{(i)} & d_{16}^{(i)} & d_{16}^{(i)} & \varepsilon_{11}^{(i)} & \varepsilon_{12}^{(i)} & \varepsilon_{13}^{(i)} \\
d_{21}^{(i)} & d_{22}^{(i)} & d_{23}^{(i)} & d_{24}^{(i)} & d_{24}^{(i)} & d_{25}^{(i)} & d_{26}^{(i)} & d_{26}^{(i)} & \varepsilon_{12}^{(i)} & \varepsilon_{22}^{(i)} & \varepsilon_{23}^{(i)} \\
d_{31}^{(i)} & d_{32}^{(i)} & d_{33}^{(i)} & d_{34}^{(i)} & d_{34}^{(i)} & d_{35}^{(i)} & d_{36}^{(i)} & d_{36}^{(i)} & \varepsilon_{13}^{(i)} & \varepsilon_{23}^{(i)} & \varepsilon_{33}^{(i)}
\end{pmatrix}$$

(2.12)
$$b^{(i)} = \begin{pmatrix}
s_{11}^{(i)} & s_{12}^{(i)} & s_{13}^{(i)} & s_{14}^{(i)} & s_{14}^{(i)} & s_{15}^{(i)} & s_{16}^{(i)} & s_{16}^{(i)} & d_{11}^{(i)} & d_{21}^{(i)} & d_{31}^{(i)} \\
0 & 1 & 0 & 0 & 0 & 0 & 0 & 0 & 0 & 0 & 0 \\
s_{13}^{(i)} & s_{23}^{(i)} & s_{33}^{(i)} & s_{34}^{(i)} & s_{34}^{(i)} & s_{35}^{(i)} & s_{36}^{(i)} & s_{36}^{(i)} & d_{13}^{(i)} & d_{23}^{(i)} & d_{33}^{(i)} \\
0 & 0 & 0 & 1 & 0 & 0 & 0 & 0 & 0 & 0 & 0 \\
s_{14}^{(i)} & s_{24}^{(i)} & s_{34}^{(i)} & s_{44}^{(i)} & s_{44}^{(i)} & s_{45}^{(i)} & s_{46}^{(i)} & s_{46}^{(i)} & d_{14}^{(i)} & d_{24}^{(i)} & d_{34}^{(i)} \\
s_{15}^{(i)} & s_{25}^{(i)} & s_{35}^{(i)} & s_{45}^{(i)} & s_{45}^{(i)} & s_{55}^{(i)} & s_{56}^{(i)} & s_{56}^{(i)} & d_{15}^{(i)} & d_{25}^{(i)} & d_{35}^{(i)} \\
s_{16}^{(i)} & s_{26}^{(i)} & s_{36}^{(i)} & s_{46}^{(i)} & s_{46}^{(i)} & s_{56}^{(i)} & s_{66}^{(i)} & s_{66}^{(i)} & d_{16}^{(i)} & d_{26}^{(i)} & d_{36}^{(i)} \\
0 & 0 & 0 & 0 & 0 & 0 & 0 & 1 & 0 & 0 & 0 \\
0 & 0 & 0 & 0 & 0 & 0 & 0 & 0 & 1 & 0 & 0 \\
d_{21}^{(i)} & d_{22}^{(i)} & d_{23}^{(i)} & d_{24}^{(i)} & d_{24}^{(i)} & d_{25}^{(i)} & d_{26}^{(i)} & d_{26}^{(i)} & \varepsilon_{12}^{(i)} & \varepsilon_{22}^{(i)} & \varepsilon_{23}^{(i)} \\
0 & 0 & 0 & 0 & 0 & 0 & 0 & 0 & 0 & 0 & 1
\end{pmatrix} \qquad i = 1,2$$

The material properties of M and b must be transformed to the same cubic coordinate system as indicated in Fig.1 before substituting them into the formula. Superscript ^{eff}, $^{(1)}$ and $^{(2)}$ describe the physical properties of effective, domain 1 and domain 2, respectively. The y-axis is perpendicular to the DW as shown in Fig.1.

Effective material properties of ferroelectrics resulting from a $m\bar{3}m \rightarrow 3m$ phase transition were calculated for a twin system consisting of polarization P^I and P^{II} divided by a (010) DW. Both $v^{(1)} \neq v^{(2)}$ and $v^{(1)} = v^{(2)}$ cases were studied.

Because no complete single crystal data for ferroelectrics with $m\bar{3}m \rightarrow 3m$ phase transition could be found in the literature we borrowed the material data of $LiNbO_3$ [48]. But we used the domain structures of $m\bar{3}m \rightarrow 3m$ phase transition to demonstrate the method [Note: $LiNbO_3$ has a $\bar{3}m \rightarrow 3m$ ferroelectric transition and only two domains with 180° DW].

$v^{(I)} \neq v^{(2)}$

In order to perform the effective material property evaluation, the tensor components of elastic constants, piezoelectric coefficients and dielectric constants were first transformed to a unified coordinate system (i.e., the cubic coordinates), then these transformed properties were put into Eqs. (2.11) - (2.12). Finally, the effective properties were calculated using Eq. (2.10) for different volume ratios. Numerical solutions show that the following relations are fulfilled within the relative errors of less than 10^{-12}.

(2.13) $s_{15}^{eff} = s_{35}^{eff}, s_{12}^{eff} = s_{23}^{eff}, s_{11}^{eff} = s_{33}^{eff},$

$s_{24}^{eff} = s_{26}^{eff}, s_{34}^{eff} = s_{16}^{eff}, s_{36}^{eff} = s_{14}^{eff}, s_{56}^{eff} = s_{45}^{eff}, s_{66}^{eff} = s_{44}^{eff}$

(2.14) $d_{23}^{eff} = d_{21}^{eff}, d_{26}^{eff} = d_{24}^{eff}, d_{31}^{eff} = d_{13}^{eff}, d_{32}^{eff} = d_{12}^{eff}, d_{33}^{eff} = d_{11}^{eff},$

$d_{34}^{eff} = d_{16}^{eff}, d_{35}^{eff} = d_{15}^{eff}, d_{36}^{eff} = d_{14}^{eff}$

(2.15) $\varepsilon_{11}^{eff} = \varepsilon_{33}^{eff}, \varepsilon_{23}^{eff} = \varepsilon_{12}^{eff}$

Numerical data verified that the symmetry of this twin structure is monoclinic m and the mirror symmetry plane is perpendicular to $[\bar{1}01]$.

$v^{(I)} = v^{(2)}$

For this case in addition to Eqs. (2.13) - (2.15) the following components become zero [36]

(2.16) $s_{15}^{eff} = s_{35}^{eff} = s_{24}^{eff} = s_{26}^{eff} = s_{34}^{eff} = s_{16}^{eff} = s_{36}^{eff} = s_{14}^{eff} = s_{56}^{eff} = s_{45}^{eff} = 0$

(2.17) $d_{23}^{eff} = d_{21}^{eff} = d_{34}^{eff} = d_{16}^{eff} = d_{36}^{eff} = d_{14}^{eff} = d_{22}^{eff} = d_{25}^{eff} = 0$

(2.18) $\varepsilon_{23}^{eff} = \varepsilon_{12}^{eff} = 0$

For twins with a charged DW oriented in (010), (110), (100) and $(\bar{1}10)$, if the volume ratio of the two domains are the same, the effective symmetry could be raised to an orthorhombic *mm2*. While for twins with neutral DW's oriented in (101), (001), (011), $(0\bar{1}1)$ and $(\bar{1}01)$, the effective symmetry can not be higher than monoclinic m.

One must remember that the macroscopic and microscopic symmetries are different in multi-domain systems. The former refers to symmetry relations between different

components of macroscopic physical properties while the latter refers to the crystal lattice structure. The low symmetry of twinned crystal increases the difficulties to fully characterize its physical properties since the number of non-zero components grows rapidly with the decreasing symmetry [49]. Number of independent material constants is different for different crystallographic classes: 11 constants for tetragonal *4mm* symmetry (6 elastic, 3 piezoelectric and 2 dielectric), 12 constants for rhombohedral *3m* symmetry (6 elastic, 4 piezoelectric and 2 dielectric), 17 constants for orthorhombic *mm2* symmetry (9 elastic, 5 piezoelectric and 3 dielectric) and 26 constants for monoclinic *m* symmetry (13 elastic, 9 piezoelectric and 4 dielectric).

As analyzed above, the effective symmetry of a twin becomes lower if the domain volume ratio deviates from 50%. We also know that this deviation is usually within a few percent for most of the materials. The question is which quantities are influenced the most by this volume ratio symmetry breaking. We used a few numerical examples to gain quantitative understanding on this issue.

Listed in Table 2.1 are some numerical results calculated by using the single crystal data of $LiNbO_3$ for the twin structure of rhombohedral *3m* system. One can see that if a component is non-zero for $v^{(1)} = 0.5$, the relative change caused by small deviation of equal volume ratio is not significant for most of the quantities, particularly the elastic properties (Fig. 4). For practical purpose, if the deviation is less than 10%, material constants could be measured under the assumption of *mm2* instead of the lower *m* symmetry. The symmetry breaking is, however, important for those components immerged from zero when the volume ratio changes from equal partition. One must use the lower symmetry if these components are of interest. The simplified symmetry approach is applicable only to twin crystals with charged DW's. Twins with neutral DW's cannot reach orthorhombic *mm2* symmetry for any volume ratio therefore they must be treated as monoclinic with symmetry group *m*.

We have also calculated two other materials resulting from $m\bar{3}m \rightarrow 4mm$ ($BaTiO_3$) [48] and from $m\bar{3}m \rightarrow mm2$ ($KNbO_3$) [50] ferroelectric phase transition. For $BaTiO_3$, the effective material properties were calculated for a twin of P^I and P^{II} in Table I.2 (Appendix I) with a DW oriented in (110). For equal volume ratio, the macroscopic symmetry of the twin is *mm2* otherwise it is monoclinic *m* (see Table 2.2).

As expected, the tensor components are either symmetric or antisymmetric with respect to $v^{(1)} = 0.5$. Non-zero components of material properties change less than 10% when the volume ratios $v^{(1)}$ changes from *0.30* to *0.70*, except ε_{11}.

For $KNbO_3$, which has a $m\bar{3}m \rightarrow mm2$ phase transition, effective material properties were calculated for a twin system of P^{III} and P^{IV} (see Table I.3 in Appendix I) with a (010) DW. The results are given in Table 2.3 for several values of the volume ratios. The macroscopic symmetry belongs to *mm2* class for equal partition, otherwise it is monoclinic *m*. The non-zero components of effective material properties d_{15}, d_{32}, d_{33} and ε_{33} change significantly with $v^{(1)}$. Therefore, one must consider monoclinic *m* symmetry while characterizing this system when $v^{(1)}$ deviates from *0.5*.

2.3 Conclusions

The effective symmetry and material properties of twin crystals have been analyzed for three symmetry classes resulting from $m\bar{3}m \rightarrow 3m$, $m\bar{3}m \rightarrow 4mm$ and $m\bar{3}m \rightarrow mm2$ ferroelectric phase transitions. It has been shown that the macroscopic symmetry could be lower than the microscopic symmetry, particularly when the volume ratios of the two domains are different. This unequal partition of domain volume leads

to a symmetry reduction in terms of macroscopic physical quantities. Numerical calculation on three real materials showed that the changes of nonzero components of the elastic, dielectric and piezoelectric quantities were not significant if the deviation from equal partition is less than 5% in the case of $m\bar{3}m \rightarrow 3m$ and $m\bar{3}m \rightarrow 4mm$, but became noticeable for the case of $m\bar{3}m \rightarrow mm2$. The symmetry reduction is signified by the appearance of several more property components when the volume ratio deviates from 50%.

Table 2.1 Effective material constants of a twinned $LiNbO_3$ single crystal versus volume ratio of domain 1 (Units: $s_{\alpha\beta}$ [10^{-12} m^2N^{-1}], $d_{i\alpha}$ [10^{-12} CN^{-1}], ε_{ij} [ε_0]). Dots (...) represent that the corresponding component is zero by symmetry and the polarization of the two domains are $P^I = P_S(111)$ and $P^{II} = P_S(1\bar{1}1)$ (Table I.1 Appendix I).

$v^{(1)}$	1.00	0.00	0.50	0.55	0.60	0.65	0.70
			Elastic Properties				
s_{11}	5.60	5.60	5.42	5.43	5.43	5.44	5.45
s_{12}	-1.36	-1.36	-1.10	-1.10	-1.11	-1.11	-1.12
s_{13}	-1.36	-1.36	-1.38	-1.38	-1.38	-1.38	-1.38
s_{14}	-1.35	1.35	...	-0.13	-0.25	-0.38	-0.51
s_{15}	0.26	0.26	-0.49	-0.48	-0.47	-0.45	-0.42
s_{16}	0.26	-0.26	...	0.03	0.06	0.09	0.12
s_{22}	5.60	5.60	4.65	4.66	4.67	4.70	4.73
s_{23}	-1.36	-1.36	-1.10	-1.10	-1.11	-1.11	-1.12
s_{24}	0.26	-0.26	...	0.00	0.00	0.01	0.02
s_{25}	-1.35	-1.35	1.36	1.35	1.30	1.23	1.13
s_{26}	0.26	-0.26	...	0.00	0.00	0.01	0.02
s_{33}	5.60	5.60	5.42	5.43	5.43	5.44	5.45
s_{34}	0.26	-0.26	...	0.03	0.06	0.09	0.12
s_{35}	0.26	0.26	-0.49	-0.48	-0.47	-0.45	-0.42
s_{36}	-1.35	1.35	...	-0.13	-0.25	-0.38	-0.51
s_{44}	15.65	15.65	15.27	15.27	15.28	15.30	15.32
s_{45}	-0.98	0.98	...	-0.03	-0.07	-0.11	-0.16
s_{46}	-0.98	-0.98	-0.99	-0.99	-0.99	-0.99	-0.99
s_{55}	15.65	15.65	7.92	7.96	8.08	8.27	8.57
s_{56}	-0.98	0.98	...	-0.03	-0.07	-0.11	-0.16
s_{66}	15.65	15.65	15.27	15.27	15.28	15.30	15.32
			Piezoelectric properties				
d_{11}	16.28	16.28	11.84	11.88	12.01	12.22	12.52
d_{12}	-5.83	-5.83	-5.03	-5.04	-5.04	-5.06	-5.08
d_{13}	-5.83	-5.83	-3.14	-3.17	-3.25	-3.39	-3.59
d_{14}	-47.11	47.11	...	-4.59	-9.19	-13.80	-18.43
d_{15}	26.44	26.44	23.84	23.85	23.88	23.94	24.03
d_{16}	26.44	-26.44	...	2.60	5.20	7.81	10.43
d_{21}	-5.83	5.83	...	-0.34	-0.68	-1.05	-1.43
d_{22}	16.28	-16.28	...	0.77	1.56	2.41	3.34
d_{23}	-5.83	5.83	...	-0.34	-0.68	-1.05	-1.43
d_{24}	26.44	26.44	22.23	22.26	22.32	22.44	22.61
d_{25}	-47.11	47.11	...	-2.25	-4.57	-7.05	-9.78
d_{26}	26.44	26.44	22.23	22.26	22.32	22.44	22.61

d_{31}	-5.83	-5.83	-3.14	-3.17	-3.25	-3.39	-3.59
d_{32}	-5.83	-5.83	-5.03	-5.04	-5.04	-5.06	-5.08
d_{33}	16.28	16.28	11.84	11.88	12.01	12.21	12.52
d_{34}	26.44	-26.44	...	2.60	5.20	7.81	10.43
d_{35}	26.44	26.44	23.84	23.85	23.88	23.94	24.03
d_{36}	-47.11	47.11	...	-4.59	-9.19	-13.80	-18.43
			Dielectric Properties				
ε_{11}	38.97	38.97	18.97	19.20	19.77	20.78	22.14
ε_{12}	-4.97	4.97	...	-0.34	-0.79	-1.13	-1.58
ε_{13}	-4.97	-4.97	11.63	11.52	11.07	10.28	9.04
ε_{22}	38.97	38.97	21.57	21.69	22.02	22.48	23.04
ε_{23}	-4.97	4.97	...	-0.34	-0.79	-1.13	-1.58
ε_{33}	38.97	38.97	18.97	19.20	19.77	20.78	22.14

Table 2.2 Effective material constants of twinned $BaTiO_3$ crystal (Units are the same as in Table 2.1). Polarizations of the two domains are $P^I = P_S(100)$ and $P^{II} = P_S(010)$ (Table I.2 Appendix I).

$v^{(1)}$	1.00	0.00	0.50	0.55	0.60	0.65	0.70
			Elastic Properties				
s_{11}	7.92	7.92	7.49	7.49	7.51	7.52	7.55
s_{12}	-1.28	-1.28	-1.71	-1.71	-1.69	-1.68	-1.65
s_{13}	-3.80	-3.80	-3.47	-3.47	-3.48	-3.50	-3.52
s_{14}	...	...	...	...	...	...	...
s_{15}	...	...	...	...	...	...	...
s_{16}	3.83	-3.83	...	0.34	0.69	1.04	1.39
s_{22}	7.92	7.92	7.49	7.49	7.51	7.52	7.55
s_{23}	-3.80	-3.80	-3.47	-3.47	-3.48	-3.50	-3.52
s_{24}	...	...	...	...	...	...	...
s_{25}	...	...	...	...	...	...	...
s_{26}	3.83	-3.83	...	0.34	0.69	1.04	1.39
s_{33}	8.05	8.05	7.81	7.81	7.81	7.83	7.84
s_{34}	...	...	...	...	...	...	...
s_{35}	...	...	...	...	...	...	...
s_{36}	-2.89	2.89	...	-0.26	-0.52	-0.78	-1.05
s_{44}	13.62	13.62	11.94	11.96	12.00	12.08	12.18
s_{45}	4.78	-4.78	...	0.42	0.84	1.27	1.71
s_{46}	...	...	...	...	...	...	...
s_{55}	13.62	13.62	11.94	11.96	12.00	12.08	12.18
s_{56}	...	...	...	...	...	...	...
s_{66}	34.23	34.23	30.63	30.66	30.76	30.92	31.16
			Piezoelectric Properties				
d_{11}	-156.66	156.66	...	-16.14	-32.24	-48.30	-64.28
d_{12}	120.53	-120.53	...	11.58	23.19	34.85	46.59
d_{13}	24.40	-24.40	...	2.79	5.57	8.30	10.98
d_{14}	...	...	...	...	...	...	...
d_{15}	...	...	...	...	...	...	...
d_{16}	-84.92	-84.92	-127.29	-126.92	-125.77	-123.85	-121.12

d_{21}	120.53	120.53	130.02	129.93	129.68	129.44	128.63
d_{22}	-156.66	-156.66	-147.17	-147.26	-147.51	-147.94	-148.55
d_{23}	24.40	24.40	17.23	17.29	17.48	17.81	18.27
d_{24}	...	...	...	...	...	...	...
d_{25}	...	...	...	...	...	...	...
d_{26}	-84.92	84.92	...	-7.61	-15.26	-23.02	-30.92
d_{31}	...	...	...	...	...	...	...
d_{32}	...	...	...	...	...	...	...
d_{33}	...	...	...	...	...	...	...
d_{34}	-277.19	-277.19	-179.91	-180.76	-183.33	-187.67	-193.83
d_{35}	-277.19	277.19	...	-24.33	-48.85	-73.73	-99.17
d_{36}	...	...	...	...	...	...	...
			Dielectric Properties				
ε_{11}	1530	1530	272	285	322	385	472
ε_{12}	-1362	1362	...	-135	-270	-405	-541
ε_{13}	...	...	...	...	...	...	...
ε_{22}	1530	1530	1506	1506	1507	1508	1509
ε_{23}	...	...	...	...	...	...	...
ε_{33}	2891	2891	2254	2260	2277	2305	2345

Table 2.3 Effective material constants of twinned $KNbO_3$ crystal (Units are the same as in Table 2.1). The polarization of the two domain are $P^{III} = P_S(011)$ and $P^{IV} = P_S(0\bar{1}1)$ (Table I.3 Appendix I).

$v^{(1)}$	1.00	0.00	0.50	0.55	0.60	0.65	0.70
			Elastic Properties				
s_{11}	5.41	5.41	5.40	5.40	5.40	5.40	5.40
s_{12}	-1.33	-1.33	-1.35	-1.35	-1.35	-1.35	-1.35
s_{13}	-1.33	-1.33	-1.34	-1.34	-1.34	-1.34	-1.34
s_{14}	0.31	-0.31	...	0.03	0.06	0.09	0.12
s_{15}	...	...	...	...	...	...	...
s_{16}	...	...	...	...	...	...	...
s_{22}	5.28	5.28	5.20	5.20	5.20	5.21	5.21
s_{23}	-1.45	-1.45	-1.49	-1.49	-1.49	-1.49	-1.49
s_{24}	0.97	-0.97	...	0.10	0.19	0.29	0.39
s_{25}	...	...	...	...	...	...	...
s_{26}	...	...	...	...	...	...	...
s_{33}	5.28	5.28	5.21	5.21	5.21	5.21	5.22
s_{34}	0.97	-0.97	...	0.10	0.19	0.29	0.38
s_{35}	...	...	...	...	...	...	...
s_{36}	...	...	...	...	...	...	...
s_{44}	16.46	16.46	16.22	16.22	16.23	16.24	16.26
s_{45}	...	...	...	...	...	...	...
s_{46}	...	...	...	...	...	...	...
s_{55}	25.24	25.24	16.60	16.65	16.83	17.13	17.56
s_{56}	14.76	-14.76	...	0.97	1.97	3.01	4.11
s_{66}	25.24	25.24	16.60	16.65	16.83	17.13	17.56
			Piezoelectric Properties				
d_{11}	...	...	...	...	...	...	...

d_{12}	...	...	...	...	...	...	...
d_{13}	...	...	...	...	...	...	...
d_{14}	...	...	...	...	...	...	...
d_{15}	72.83	72.83	30.22	30.50	31.36	32.82	34.96
d_{16}	72.83	-72.83	...	4.81	9.71	14.83	20.27
d_{21}	7.00	-7.00	...	0.71	1.41	2.12	2.82
d_{22}	31.57	-31.57	...	3.17	6.35	9.52	12.69
d_{23}	-23.58	23.58	...	-2.33	-4.66	-6.99	-9.33
d_{24}	35.14	35.14	39.37	39.33	39.20	39.00	38.70
d_{25}	...	...	...	...	...	...	...
d_{26}	...	...	...	...	...	...	...
d_{31}	7.00	7.00	12.14	12.09	11.93	11.67	11.31
d_{32}	-23.58	-23.58	1.41	1.16	0.40	-0.86	-2.62
d_{33}	31.57	31.57	5.95	6.20	6.96	8.23	10.00
d_{34}	35.14	-35.14	...	3.03	6.06	9.21	12.42
d_{35}	...	...	...	...	...	...	...
d_{36}	...	...	...	...	...	...	...
			Dielectric Properties				
ε_{11}	1540	1540	1516	1516	1517	1518	1519
ε_{12}	...	...	...	...	...	...	...
ε_{13}	...	...	...	...	...	...	...
ε_{22}	5145	5145	5133	5133	5133	5134	5135
ε_{23}	-4705	4705	...	-469	-939	-1408	-1878
ε_{33}	5145	5145	811	854	984	1200	1503

Figure1a,b. Twin system symmetry in $m\bar{3}m \rightarrow 3m$ ferroelectrics. Twinned system calculated in Table 2.1 is in Fig.1a. Volume ratio $v^{(1)}=1.00$ is for domain $P^{I} = P_S(111)$, $v^{(1)}=0.00$ is for domain $P^{II} = P_S(1\bar{1}1)$.

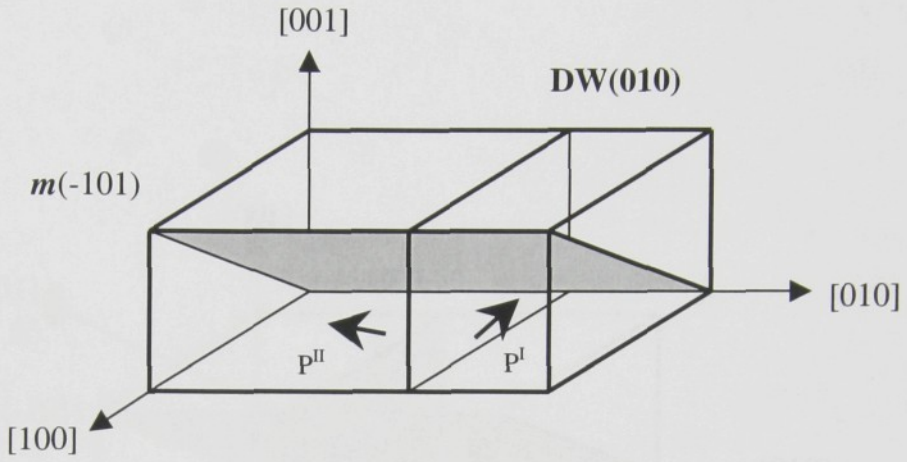

a)

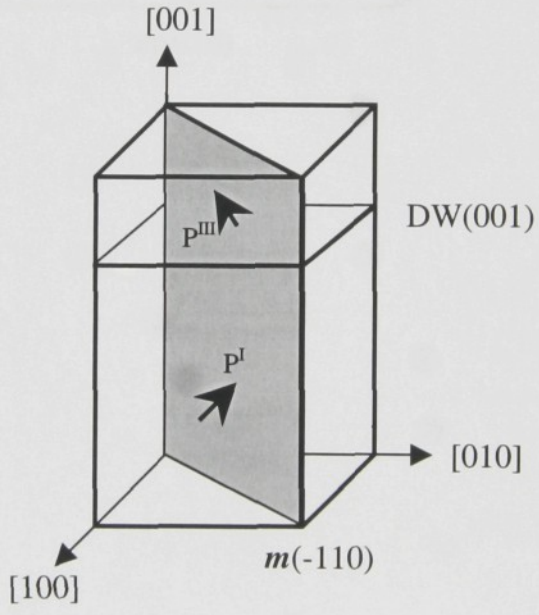

b)

Figure1c. Twin system symmetry in $m\bar{3}m \rightarrow 3m$ ferroelectrics. Volume ratio $v^{(1)}=1.00$ is for domain $P^{I} = P_S(111)$, $v^{(1)}=0.00$ is for domain $P^{II} = P_S(1\bar{1}1)$.

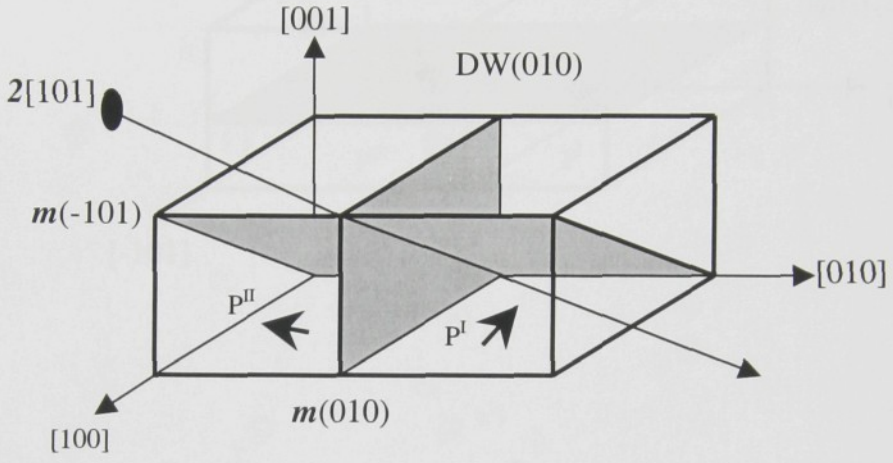

c)

Figure 2a,b. Twin system symmetry in $m\bar{3}m \rightarrow 4mm$ ferroelectrics. Effective macroscopic symmetry is ***m***.

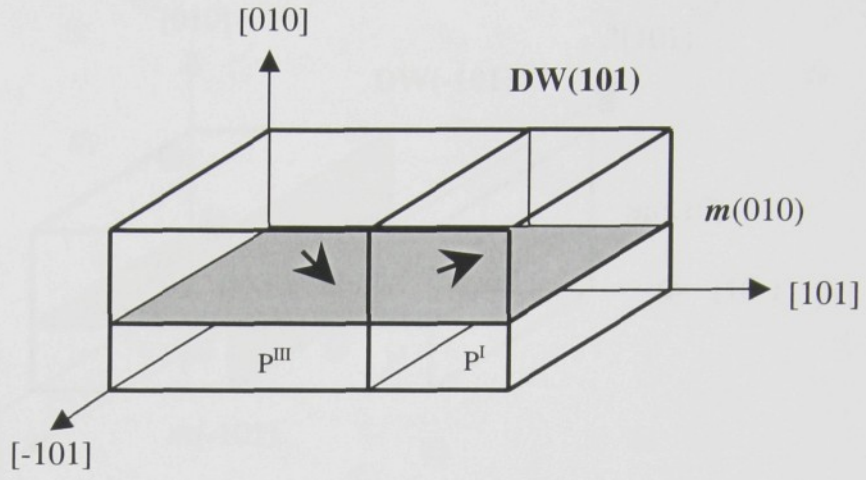

a)

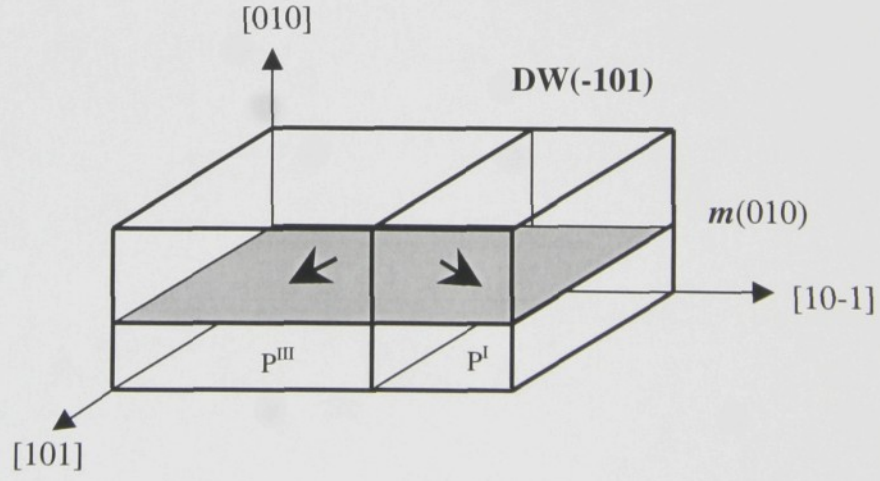

b)

Figure 2c. Twin system symmetry in $m\bar{3}m \rightarrow 4mm$ ferroelectrics. Effective macroscopic symmetry is ***mm2***.

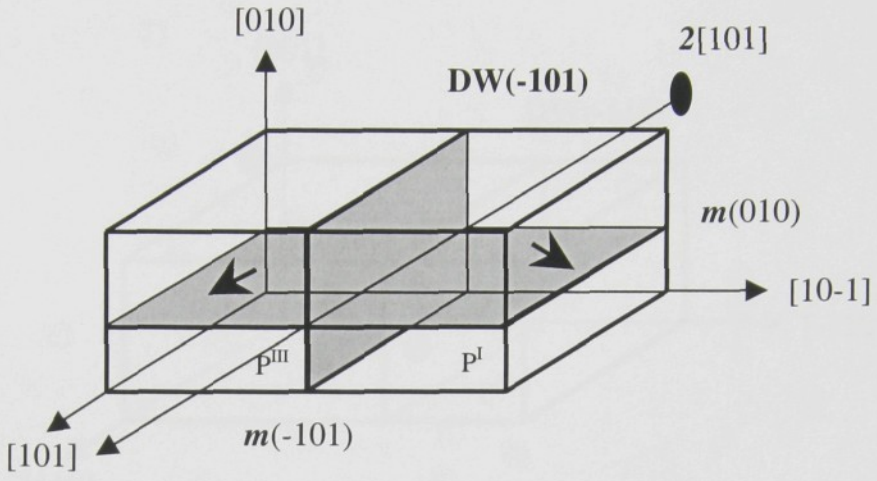

c)

Figure 3a,b. Twin system symmetry in $m\bar{3}m \rightarrow mm2$ ferroelectrics. Volume ratio $v^{(1)}=1.00$ is for domain $P^{III} = P_S(011)$, $v^{(1)} = 0.00$ is for domain $P^{IV} = P_S(0\bar{1}1)$. Effective macroscopic symmetry is either ***m*** or ***1***.

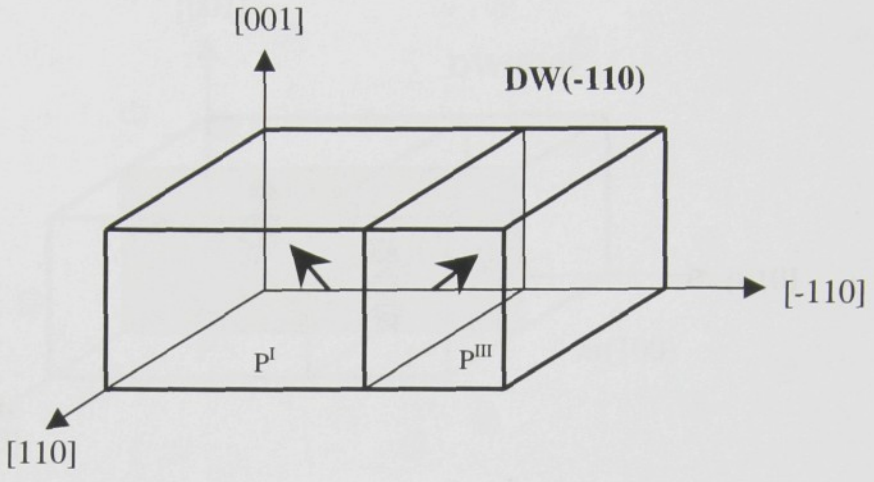

a)

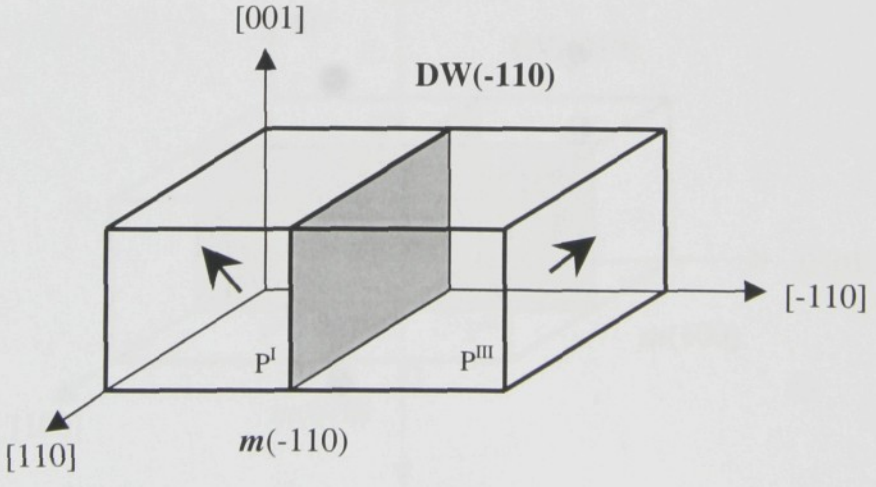

b)

Figure 3c,d. Twin system symmetry in $m\bar{3}m \rightarrow mm2$ ferroelectrics. Twinned system calculated in Table 2.3 is in Fig.3c. Volume ratio $v^{(1)}=1.00$ is for domain $P^{III} = P_S(011)$, $v^{(1)} = 0.00$ is for domain $P^{IV} = P_S(0\bar{1}1)$. Effective macroscopic symmetry is either ***m*** or ***mm2***.

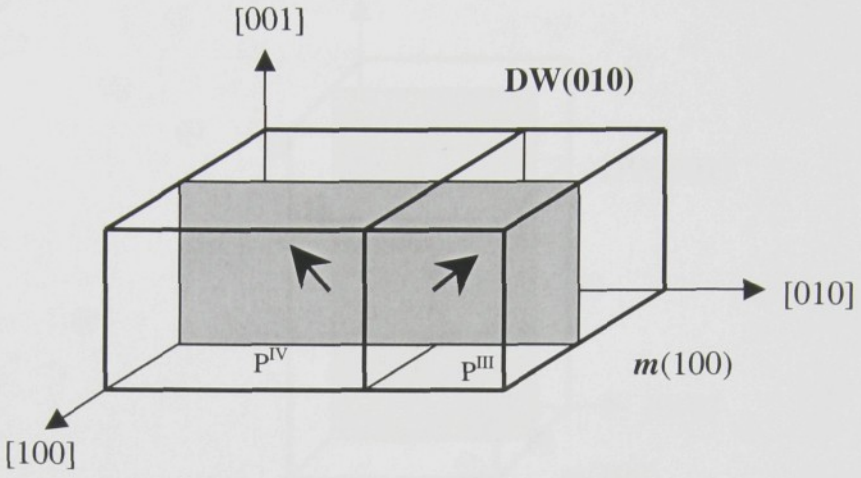

c)

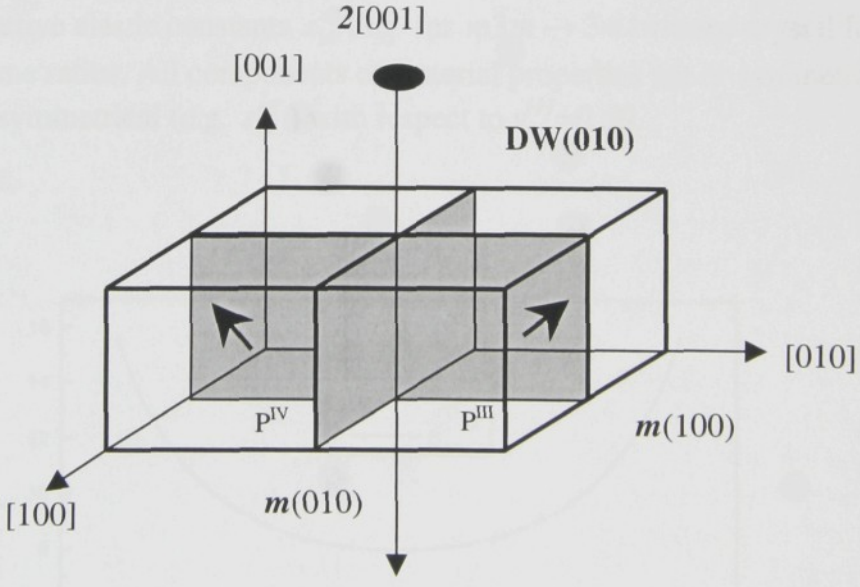

d)

Figure 3e. Twin system symmetry in $m\bar{3}m \rightarrow mm2$ ferroelectrics. Volume ratio $v^{(1)}=1.00$ is for domain $P^{III} = P_S(011)$, $v^{(1)} = 0.00$ is for domain $P^{IV} = P_S(0\bar{1}1)$. Effective macroscopic symmetry is ***m***.

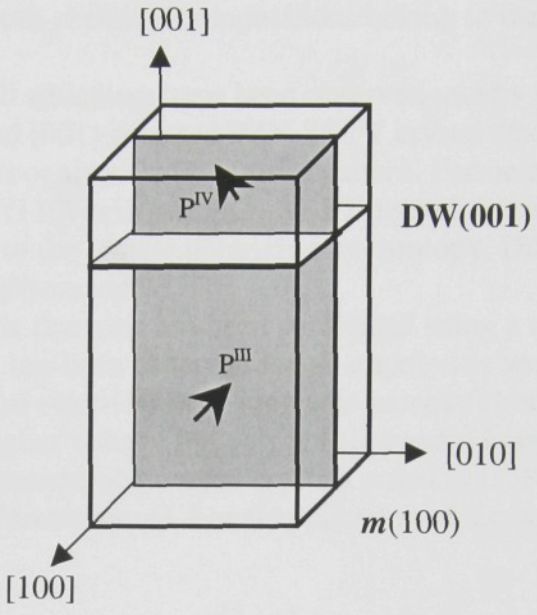

e)

Figure 4. Effective elastic constants $s_{14}^{eff}, s_{55}^{eff}$ for $m\bar{3}m \rightarrow 3m$ twinned crystal for different volume ratios. All components of material properties are or symmetrical (e.g. s_{55}^{eff}) or asymmetrical (e.g. s_{14}^{eff}) with respect to $v^{(1)}=0.50$.

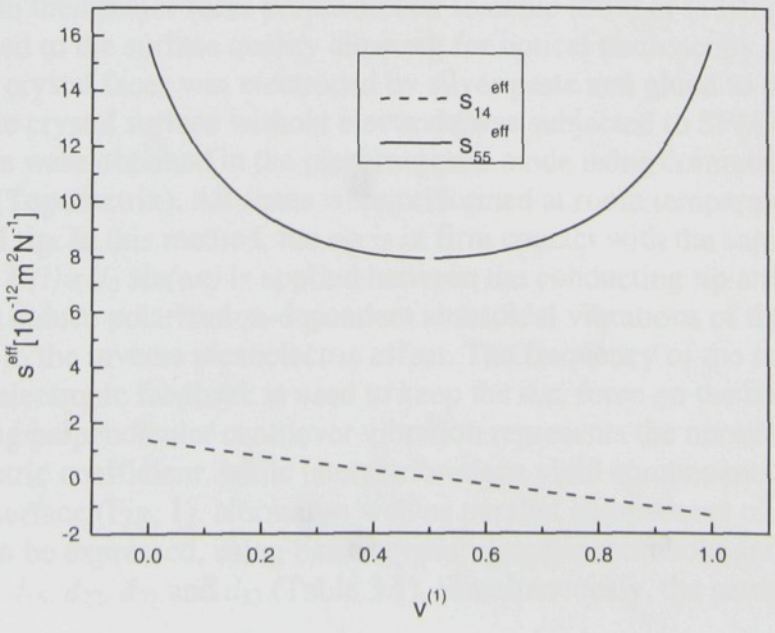

3. Domain structure observations in PZN-PT and PMN-PT crystals

In this chapter, our own domain structure observations [43,44] of unpoled as well as poled (along [001]- and [110]-direction) PZN-8%PT and PMN-29%PT single-crystals done by the piezoresponse mode scanning force microscopy (SFM) at room temperature are reported. Both chemical compositions belong to the rhombohedral phase near MPB.

Antiparallel domain wall structures have been observed mostly in unpoled crystals of both materials. In unpoled (001)-oriented PZN-8%PT crystal also preferred domain wall directions have been recognized in fingerprint pattern. Ferroelastic domain wall has been observed in poled (110)-oriented PZN-8%PT crystal. Piezoresponse mode SFM images are correlated to the optical polarizing microscopy. Different scale of the observed domain pattern is discussed.

"Writing" of ferroelectric domains has been performed using a d.c. voltage applied at SFM tip. Local re-poling has been observed for all unpoled as well as for poled (001)-oriented crystals. Local electrical switching was successful in poled (110)-oriented PMN-29%PT at higher voltage but was not successful in poled (110)-oriented PZN-8%PT crystal at all. Domain-engineered crystals poled in [110]-direction seem to exhibit more stable domain arrangement. Local application of a.c. voltage resulted in local hysteresis loops.

3.1 Experimental method

PZN-PT and PMN-PT single-crystals were provided by Crystal Associates, Inc., East Hanover, NJ, USA. Crystals of PZN-PT were grown by method of spontaneous nucleation and slow cooling. In this method the solution of PbO flux and PZN-PT are heated until the entire solution is molten and then cooled through the saturation temperature to create nuclei which grow as the solution is further cooled. Many crystals of varying size are grown by this method. The amount of PT in the solid solution is always very close to that in the starting mixture.

PZN-8%PT and PMN-29%PT have a chemical composition, which at room temperature corresponds to rhombohedral ferroelectric phase close to the MPB. Square plates (5 x 5 mm^2 with thickness ranging from 0.39 to 0.89 mm) used in this work were oriented with their major faces perpendicular to cubic (001) or (110) plane. Samples were polished to the surface quality allowing for optical microscopy observations. One of the main crystal faces was electroded by silver paste and glued to the SFM holder. The opposite crystal surface without electrode was subjected to SFM tip scanning. SFM images were obtained in the piezoresponse mode using commercially available equipment (Topometrix). All scans were performed at room temperature with a doped silicon SFM tip. In this method, the tip is in firm contact with the sample surface. An a.c. voltage $U(t)=U_0 \sin(\omega t)$ is applied between the conducting tip and the counter electrode to induce polarization-dependent sinusoidal vibrations of the ferroelectric sample due to the inverse piezoelectric effect. The frequency of the a.c. voltage was *20kHz*. An electronic feedback is used to keep the d.c. force on the cantilever constant. The resulting perpendicular cantilever vibration represents the normal component ($d_\perp$) of piezoelectric coefficient, while lateral vibrations yield components parallel ($d_{\parallel 1}$ or $d_{\parallel 2}$) to the surface (Fig. 1). Normal as well as parallel components of the piezoelectric response can be expressed, using basic crystallographic rhombohedral piezoelectric coefficients d_{15}, d_{22}, d_{31} and d_{33} (Table 3.1). Simultaneously, the sample surface

topography is recorded so that any influence of the surface morphology can be analyzed.

Table 3.1 Components of the piezoelectric coefficient parallel and perpendicular to the crystal surface for permissible domain states in the rhombohedral ferroelectric phase. Contrast of the measured response in the piezoresponse mode SFM corresponds to the listed components.

	(001)			(110)		
	$d_{\perp}$	$d_{\parallel 1}$	$d_{\parallel 2}$	$d_{\perp}$	$d_{\parallel 1}$	$d_{\parallel 2}$
P^{I}	$+d_{11}^{eff}$	$+d_{15}^{eff}$	$+d_{15}^{eff}$	$+d_{11}^{eff}$	0	$+d_{15}^{eff<1>}$
P^{II}	$+d_{11}^{eff}$	$-d_{15}^{eff}$	$+d_{15}^{eff}$	0	$-d_{16}^{eff}$	$+d_{15}^{eff<2>}$
P^{III}	$+d_{11}^{eff}$	$-d_{15}^{eff}$	$-d_{15}^{eff}$	$-d_{11}^{eff}$	0	$+d_{15}^{eff<1>}$
P^{IV}	$+d_{11}^{eff}$	$+d_{15}^{eff}$	$-d_{15}^{eff}$	0	$+d_{16}^{eff}$	$+d_{15}^{eff<2>}$
P^{V}	$-d_{11}^{eff}$	$-d_{15}^{eff}$	$-d_{15}^{eff}$	$-d_{11}^{eff}$	0	$-d_{15}^{eff<1>}$
P^{VI}	$-d_{11}^{eff}$	$+d_{15}^{eff}$	$-d_{15}^{eff}$	0	$+d_{16}^{eff}$	$-d_{15}^{eff<2>}$
P^{VII}	$-d_{11}^{eff}$	$+d_{15}^{eff}$	$+d_{15}^{eff}$	$+d_{11}^{eff}$	0	$-d_{15}^{eff<1>}$
P^{VIII}	$-d_{11}^{eff}$	$-d_{15}^{eff}$	$+d_{15}^{eff}$	0	$-d_{16}^{eff}$	$-d_{15}^{eff<2>}$
	$d_{11}^{eff} = \frac{\sqrt{3}}{9}\left(2d_{15} - 2\sqrt{2}d_{22} + 2d_{31} + d_{33}\right)$ $d_{15}^{eff} = \frac{\sqrt{3}}{9}\left(d_{15} + 2\sqrt{2}d_{22} - 2d_{31} + 2d_{33}\right)$			$d_{11}^{eff} = \frac{\sqrt{6}}{18}\left(2d_{15} + \sqrt{2}d_{22} + 2d_{31} + 4d_{33}\right)$ $d_{15}^{eff\langle 1\rangle} = \frac{\sqrt{3}}{9}\left(-d_{15} - 2\sqrt{2}d_{22} - 4d_{31} + 4d_{33}\right)$ $d_{15}^{eff\langle 2\rangle} = \frac{\sqrt{3}}{3}\left(d_{15} + 2\sqrt{2}d_{22}\right)$ $d_{16}^{eff} = \frac{\sqrt{6}}{3}\left(d_{15} - \sqrt{2}d_{22}\right)$		

In addition to passive observations, the SFM method in the contact mode offers another very useful investigative tool, namely a locally induced switching process. If a d.c. voltage is applied to the tip, sample could be locally poled and this will be analyzed in subsequent SFM scan. This offers an easy way to check whether the observed pattern really corresponds to ferroelectric domains.

3.2 Results and discussion

Rhombohedral ferroelectric phase allows for the existence of 8 domain states (for complete set of all permissible domain wall orientations see Appendix I) with spontaneous polarization vectors oriented in the directions of cube diagonals of the parent cubic phase, i.e.

$$P^{I} = \frac{1}{\sqrt{3}} P_S(111),\ P^{II} = \frac{1}{\sqrt{3}} P_S(1\bar{1}1),\ P^{III} = \frac{1}{\sqrt{3}} P_S(\bar{1}\bar{1}1),\ P^{IV} = \frac{1}{\sqrt{3}} P_S(\bar{1}11), \quad (3.1a)$$

$$P^{V} = \frac{1}{\sqrt{3}} P_S(\bar{1}\bar{1}\bar{1}),\ P^{VI} = \frac{1}{\sqrt{3}} P_S(\bar{1}1\bar{1}),\ P^{VII} = \frac{1}{\sqrt{3}} P_S(11\bar{1}),\ P^{VIII} = \frac{1}{\sqrt{3}} P_S(1\bar{1}\bar{1}). \quad (3.1b)$$

Among all permissible domain wall orientations in $m\bar{3}m \rightarrow 3m$ ferroelectric species there are 180°-domain walls with arbitrary crystallographic orientations or ferroelastic domain walls of {110}- and {100}-type. No S-walls are permissible in this ferroelectric species.

3.2.1 (001) oriented samples

Domain-engineered crystal structure has been generated in these crystal cuts by poling in [001]-direction. This direction does not belong to any of the permissible spontaneous polarization orientations in rhombohedral phase.

PZN-8%PT

Domain structure of an unpoled (001)-oriented PZN-8%PT single-crystal has been studied. Typically, fingerprint patterns (for details see [43]) have been observed such as shown in Fig. 2. In the SFM picture corresponding to the normal piezoelectric component, parallel stripes appear with a pronounced contrast. While the domain contours are not as clear as in normal ferroelectrics like $BaTiO_3$, these fingerprint patterns can be without any doubt interpreted as domains with antiparallel polarization. Domain wall contours appear very diffuse and irregular, however with preferred domain wall orientation. The domain wall preferred direction changes between two orientations (details in [43]). Typical width of antiparallel domains, as analyzed from the SFM pictures, amounts from *1* to *2* μm. The domain regions do not represent uniform domains but appear to be composed from the mixture of small regions of both antiparallel domains. Macroscopically long ferroelastic domain walls are also observed optically in unpoled crystal (Fig. 3).

Piezoelectric mode SFM scan on (001)-oriented poled PZN-8%PT sample is shown in Fig.4. SFM image contrast is shifted to one color (black), even so we see black and white structures. White areas correspond to approximately zero piezoelectric response. They could be interpreted as antiparallel domains whose remained even though the sample was poled. Poling was done at room temperature at the electric field of *0.4 kV/mm,* i.e. much lower than the value *4 kV/mm* reported previously [8]. Nor ferroelastic domain walls, nor preferred directions of antiparallel domain walls are clearly observed. Mixture of tiny domain pattern regions has been observed by optical microscopy (Fig. 5).

PMN-29%PT

Domain structure of an unpoled (001)-oriented PMN-29%PT single-crystal has been studied. System of antiparallel domains has been found. The structure is comprised of larger prevailingly uniform areas connected by thin snaky stripes (Fig. 6). Compared to PZN-8%PT crystals, their preferred direction is not clearly detectable. Typical width of thin antiparallel domains, as analyzed from SFM pictures, amounts from *0.1* to *0.2* μm. Width of the larger nearly uniform areas is greater than *0.8* μm.

Very thin and macroscopically long domains are observed by the optical microscopy (Fig. 7). Nor ferroelastic domain walls, nor preferred directions of antiparallel domain walls are clearly observed by piezoresponse SFM.

We have investigated also a poled (001)-oriented PMN-29%PT single-crystal. The domain structure observed by piezoresponse SFM is shown in Fig. 8. We can see that the sample was not fully poled by the electric field applied (*0.4 kV/mm*). Thin antiparallel domains remained after poling, however the contrast is shifted to one of the antiparallel domain states. Corresponding change in the density of domains and domain walls is observed by the optical microscopy (Fig. 9).

3.2.2 (110) oriented samples

Domain-engineered crystal structure has been generated in these crystal cuts by poling in [110]-direction. This direction does not belong to any of the permissible spontaneous polarization orientation in rhombohedral phase.

PZN-8%PT

In an unpoled (110)-oriented PZN-8%PT sample we have found two different types of images – black and white areas of antiparallel domains (P^{I} and P^{V} or P^{III} and P^{VII}) and gray areas of domains (P^{II}, P^{IV}, P^{VI} and P^{VIII}). In the first type of domain structure (Fig. 10) irregular oblong antiparallel domains exist. The width of these domains is approximately *10 μm*, in contrast to *1 μm* for (001)-cut. Grey stripe (Fig. 10 - normal response, upper left corner) is comprised of small antiparallel domains (see detail in Fig. 11). After heating and annealing (at the temperature of *470K* for several hours), the latter type of domain structure has been observed. No antiparallel domains P^{I} and P^{V} or P^{III} and P^{VII} have been found after heating. Domains P^{II}, P^{IV}, P^{VI} and P^{VIII} are not distinguishable in normal piezoelectric response and unfortunately an in-plane signal was full of noise. Regions with the mixture of tiny domains as well as macroscopically long straight ferroelastic domain walls have been observed by optical microscopy (Fig. 12) before heating. After heating, no clear domains have been observed by optical microscopy except some domain remnants at the crystal edges.

Applying d.c. voltage to SFM tip, we have succeeded in "writing" domains: positive and negative SFM contrast regions were created on the crystal surface. We tried to apply d.c. voltage to SFM tip, which was slowly changed (*0 V...+60 V...0 V... -60 V...0V*, step *5 V*). This experiment was stopped after several cycles at the voltage *+60 V*. After this experiment a black region with a polarization P^{I} or P^{V} was observed (Fig. 13). Inside this region we applied d.c. voltage *–60 V* to SFM tip (one pulse, *5 s*) and antiparallel domain appeared. It shows clearly ferroelectric nature of the observed pattern.

For a poled (110)-oriented sample only P^{I} or P^{VII} domains should be observed. These domains are indistinguishable in normal piezoelectric response and an in-plane signal was full of noise. No structure of remnants of antiparallel domains is observed at all. Weak contrast is observed at the ferroelastic domain wall either with (0-11) or (101) orientation (added white diagonal lines in Fig. 14). Corresponding domain pairs are P^{I} and P^{II} (or P^{I} and P^{VI}) for (101) domain wall and P^{II} and P^{VII} (or P^{VI} and P^{VII}) for (0-11) domain wall. Unfortunately, no contrast appears for in-plane piezoresponse signal and the domain pair could not be further specified. Optical microscopy reveals sharp and macroscopically long ferroelastic domain walls (Fig. 15) whose were not fully confirmed in piezoresponse SFM observations.

Poling experiment using SFM tip is shown in Fig. 16. We can create an antiparallel domain by applying a d.c. voltage in the direction opposite to the poling field. Depth of this domain is less than SFM detectable region, so the resultant piezoelectric signal is close to zero, i.e. SFM contrast reflects a superposition of both antiparallel domains.

PMN-29%PT

Domain structure of an unpoled (110)-oriented PMN-29%PT single-crystal has been studied. System of antiparallel domains has been observed. Their structure is comprised of larger prevailingly uniform areas and areas with tiny domains (Fig. 17). The nearly uniform areas are greater (typically from *5* to *10* μm) than in (001)-oriented PMN-29%PT (compare Figs. 6 and 17). Neither ferroelastic domain walls nor preferred direction of the antiparallel domain walls have been found. Optical microscopy does not reveal macroscopic ferroelastic domain wall structure (Fig. 18).

Applying a d.c. voltage of *±60 V* to SFM tip, we have created domains on the crystal surface. All observed domain types can be rewritten (Fig. 19). It shows ferroelectric nature of the observed pattern.

Domain structure of a poled (110)-oriented PMN-29%PT single-crystal has been also studied. Practically no structural information has been gained from the poled crystal in this orientation (mainly due to the noise). No domain pattern has been recognised. That would suggest or nearly single-domain crystal state, which was not confirmed by the optical microscopy (Fig.20) or very tiny domains distributed uniformly over the crystal surface.

3.2.3 Local hysteresis curves

SFM method in contact mode makes local poling processes possible. If a d.c. voltage is applied to the tip, sample could be locally and non-homogeneously poled. We tried to apply d.c. voltage to SFM tip, which was changed (*-60 V...0 V...+60 V... 0 V...-60V*, step *3 V*) in cycles with 3.6 mHz frequency, and to measure normal piezoelectric response (frequency of an a.c. voltage was 20 kHz). Corresponding hysteresis loops are shown in Fig. 21 (unpoled samples) and in Fig. 22 (poled samples). All unpoled samples of (001)- and (110)-oriented PZN-8%PT and PMN-29%PT single-crystals can be locally re-poled by applying d.c. voltage of *±60 V* to the SFM tip (see Fig. 13 for (110) PZN-8%PT unpoled sample). Nice hysteresis loops are observed. Poled (001)-oriented PZN-8%PT and PMN-29%PT single-crystals can be also electrically re-poled by applying d.c. voltage of *±60 V* at SFM tip. PMN-29%PT shows higher local piezoresponse (corresponding to remanent polarization) than PZN-8%PT, while local equivalent of coercive field is almost the same for both materials. Low-fatigue switching behavior has been reported previously for poled (001)-oriented PZN-PT single-crystals on macroscopic samples [30].

Poled (110)-oriented PZN-8%PT and PMN-29%PT single-crystals cannot be electrically switched by applying d.c. voltage of *±60 V*, while an application of higher *±120 V* d.c. voltage enables re-poling of a poled (110)-oriented PMN-29%PT single-crystal. Poled (110)-oriented PZN-8%PT single-crystal cannot be electrically switched even by higher electric field *±120 V* at SFM tip. This is probably a consequence of higher Curie temperature for PZN-8%PT than for PMN-29%PT, i.e. domain structure is more stable further away from the Curie temperature.

3.3 Conclusions

Domain-engineered patterns have been observed in [001]- and [110]-poled PZN-8%PT and PMN-29%PT single-crystals by piezoresponse SFM and by optical microscopy. For comparison, also domain structures of unpoled (001)- and (110)-oriented PZN-8%PT and PMN-29%PT single-crystals have been investigated.

Unpoled crystals of PZN-8%PT and PMN-29%PT show usually complicated pattern of antiparallel domain (or fingerprint structure, or other textures) in piezoresponse SFM observations. Typical dimensions of the structures observed ranges from *0.1* to *10* μm and are smaller in PMN-29%PT than in PZN-8%PT single-crystals. (001)-oriented crystals exhibited typical dimensions of the antiparallel domain structure one order of magnitude smaller than (110)-oriented PZN-8%PT and PMN-29%PT single-crystals. Preferred orientation of antiparallel domain walls has been observed moreover in (001)-oriented PZN-8%PT crystal. Observed antiparallel domain walls are not sharp and also domain regions show a mixture of nuclei of different antiparallel domains.

Poled crystals of PZN-8%PT and PMN-29%PT do not show usually a typical ferroelastic domain pattern in piezoresponse mode SFM even if it is observed by optical microscopy. It is partly due to the different scale of both methods (optical microscopy works typically over the area 1 x 1 mm^2 but SFM only over the area of 100 x 100 μm^2 or less), partly by the different imaging principles. Optical microscopy integrates light over the whole sample thickness in transmission mode but SFM covers a crystal surface and nearest neighboring layer. This is probably a reason why different domain pattern is observed by both methods. Although no regular ferroelastic domain pattern is observed in most of the poled crystals SFM contrast is shifted to the values corresponding to one of the previously present antiparallel domain states. This clearly demonstrates that the observed pattern is of ferroelectric nature. It is also further confirmed by local poling experiments done by using SFM tip in some crystals. Crystal samples were probably not fully poled using electric field of *0.4 kV/mm* except than *4 kV/mm* as previously reported in poling procedures at room temperature.

All studied unpoled single-crystals show hysteresis loops generated by applying cycles of the voltage ± 60 *V* at the SFM tip. Also poled (001)-oriented crystals exhibited hysteretic behavior at the same voltage. Poled (110)-oriented single-crystals could be electrically switched by higher voltage ± 120 *V* at SFM tip in case of PMN-29%PT, or cannot be re-poled at all by such electric field in PZN-8%PT. This would suggest that domain structure in poled (110)-oriented single-crystals is more stable than for (001)-oriented crystals.

Further SFM studies are necessary especially for poled (001)-oriented PMN-29%PT single-crystals.

Figure 1. Sample geometry with the scanning tip directions and the piezoelectric coefficients detectable by SFM.

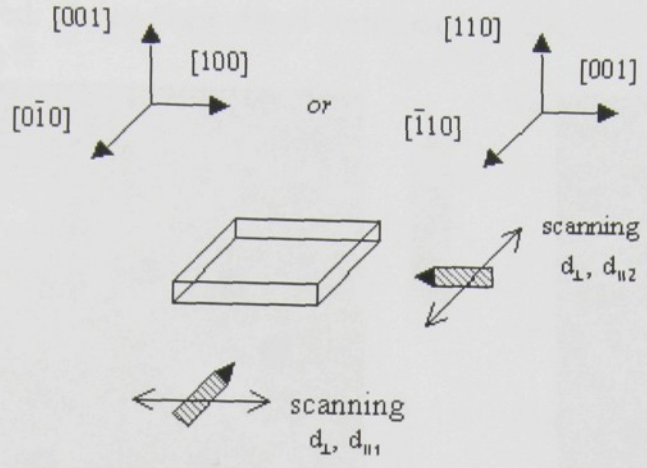

Figure 2. Piezoelectric mode SFM scan on PZN-8%PT (001) oriented unpoled sample. Topography (left) and normal (right) piezoelectric response is displayed.

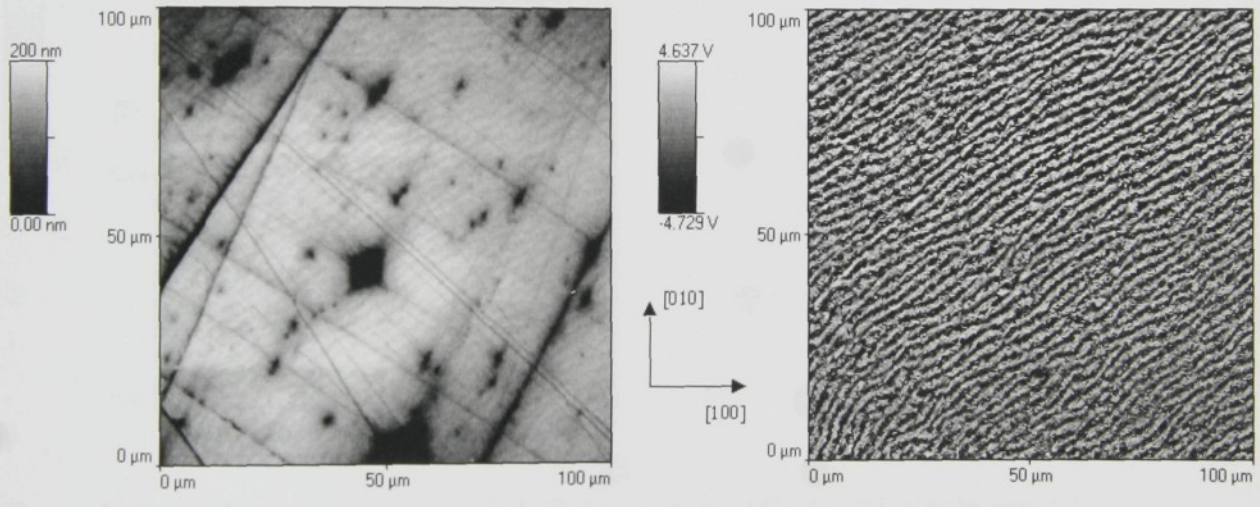

Figure 3. Optical microscopy on unpoled (001)-oriented PZN-8%PT single-crystal (edge = *1 mm*).

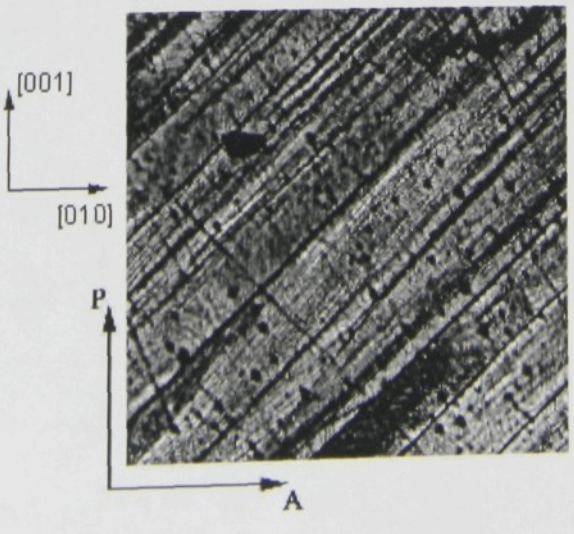

Figure 4. Piezoelectric mode SFM scan on poled (001)-oriented PZN-8%PT sample. Topography (upper left), normal (upper right) and in-plane (lower left) piezoelectric response is displayed. The in-plane signal corresponds to $d_{\parallel 1}$.

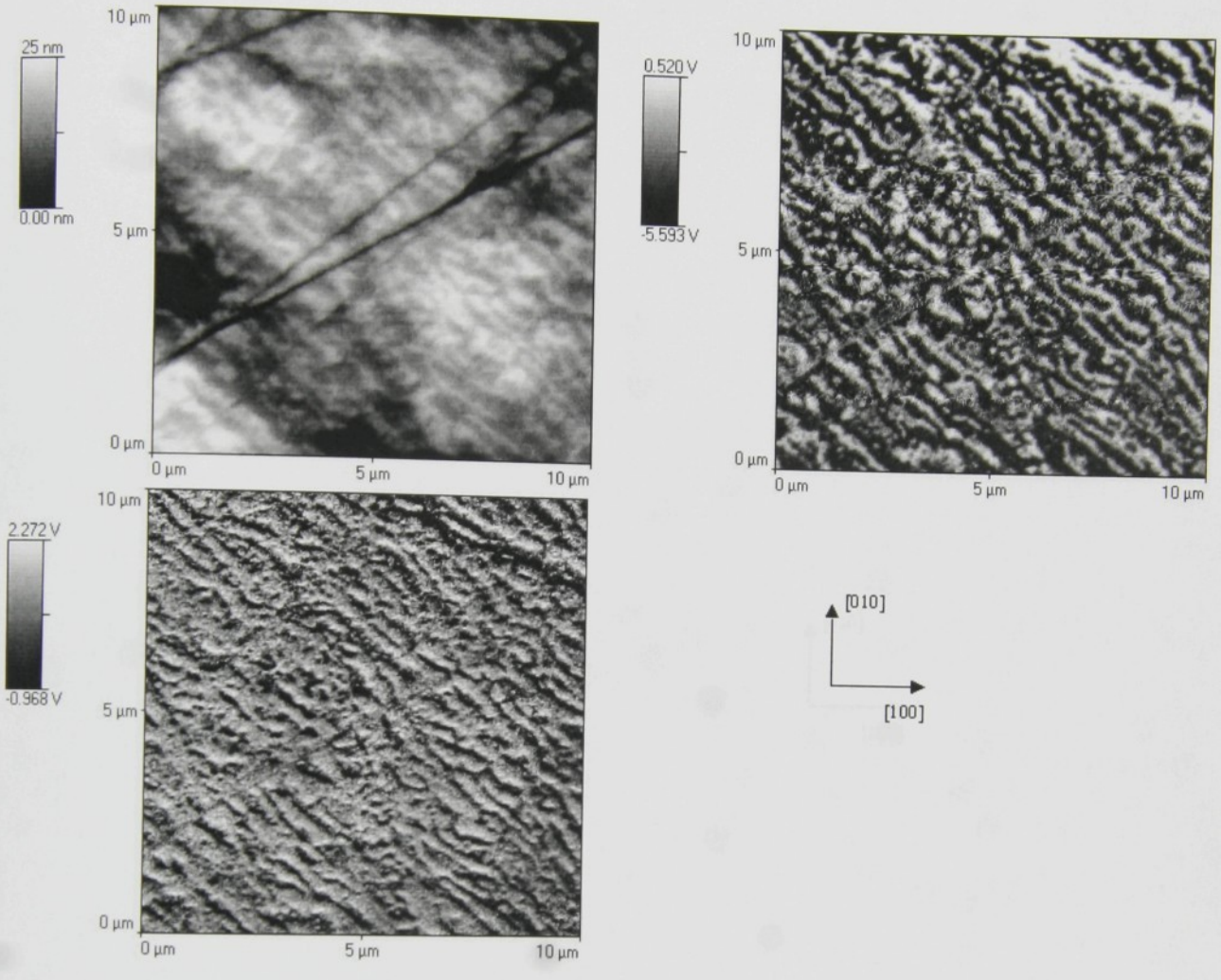

Figure 5. Optical microscopy on poled (001)-oriented PZN-8%PT single-crystal (edge = *1 mm*).

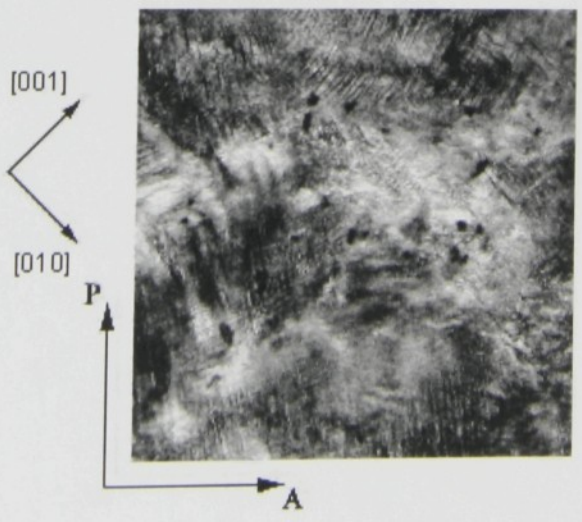

Figure 6. Piezoelectric mode SFM scan on PMN-29%PT (001) oriented unpoled sample. Topography (upper left), normal (upper right) and in-plane (lower left) piezoelectric response is displayed. The in-plane signal corresponds to $d_{\parallel 1}$.

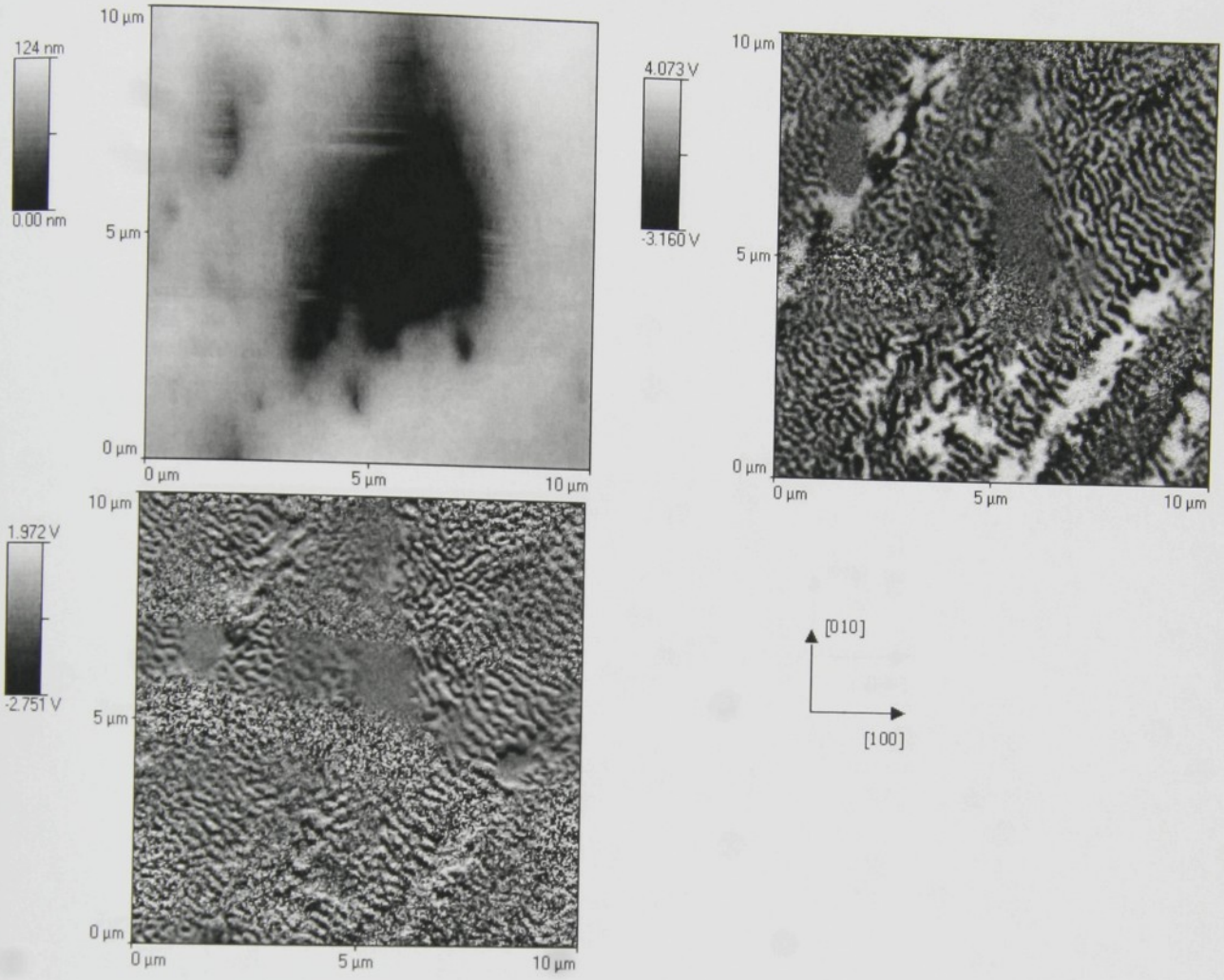

Figure 7. Optical microscopy on unpoled (001)-oriented PMN-29%PT single-crystal (edge = *1 mm*).

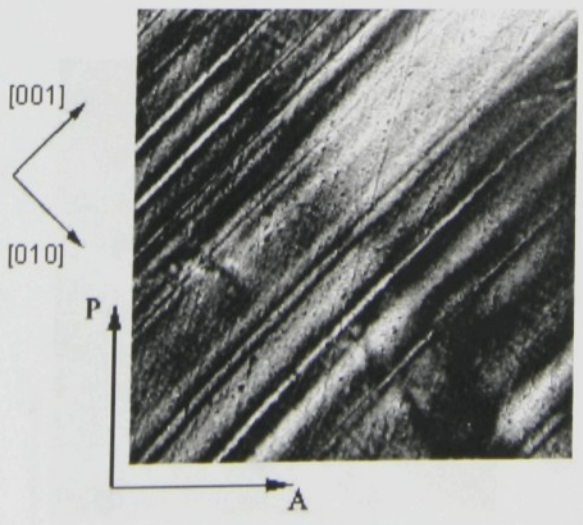

Figure 8. Piezoelectric mode SFM scan on PMN-29%PT (001) oriented poled sample. Topography (upper left), normal (upper right) and in-plane (lower left) piezoelectric response is displayed. The in-plane signal corresponds to $d_{\parallel 1}$.

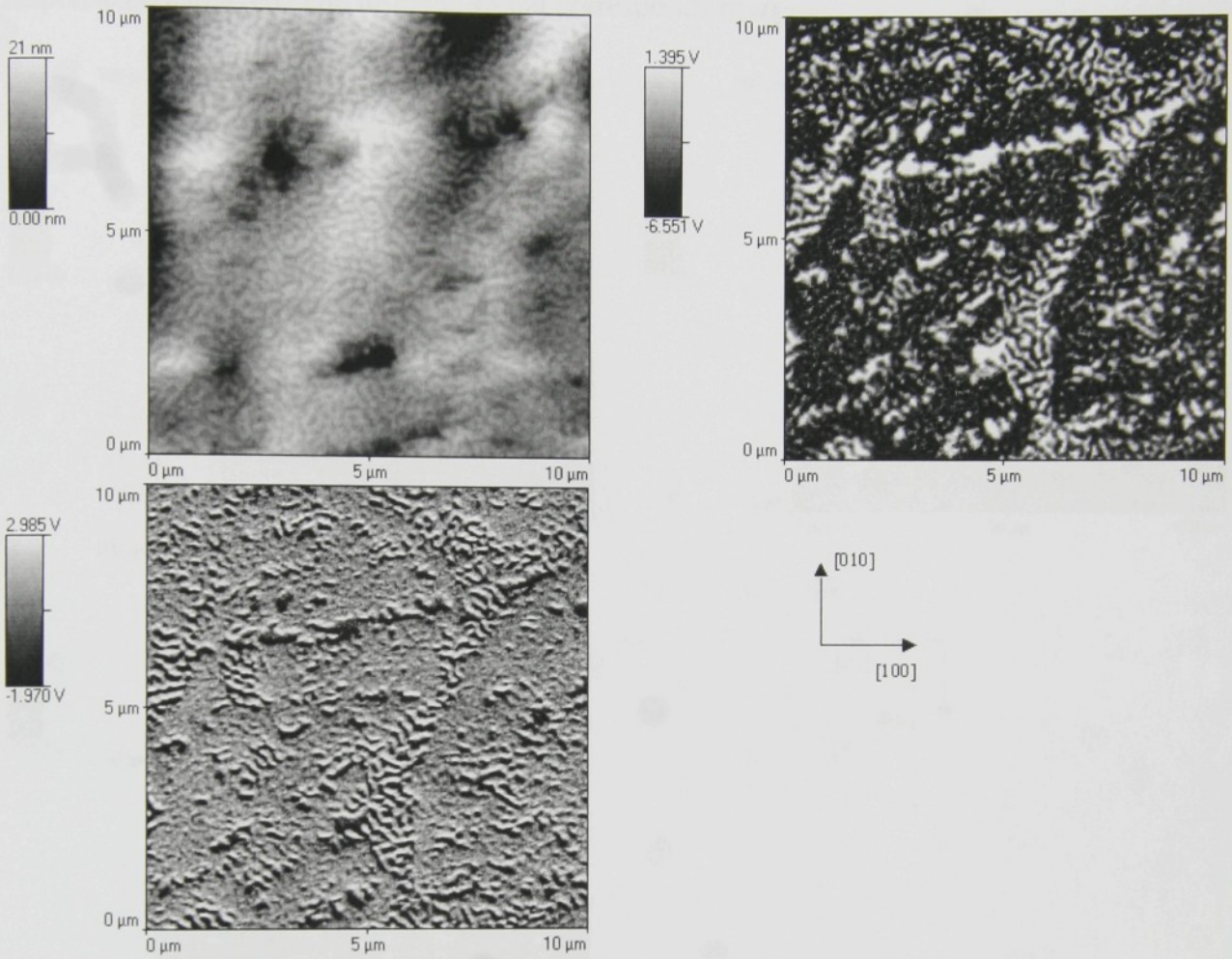

Figure 9. Optical microscopy on poled (001)-oriented PMN-29%PT single-crystal (edge=1mm).

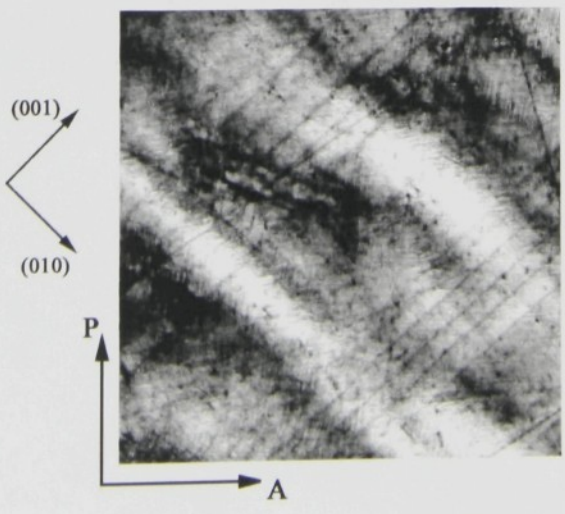

Figure 10. Piezoelectric mode SFM scan on unpoled (110)-oriented PZN-8%PT sample. Topography (upper left), normal (upper right) and in-plane (lower left) piezoelectric response is displayed. The in-plane signal corresponds to $d_{\parallel 2}$.

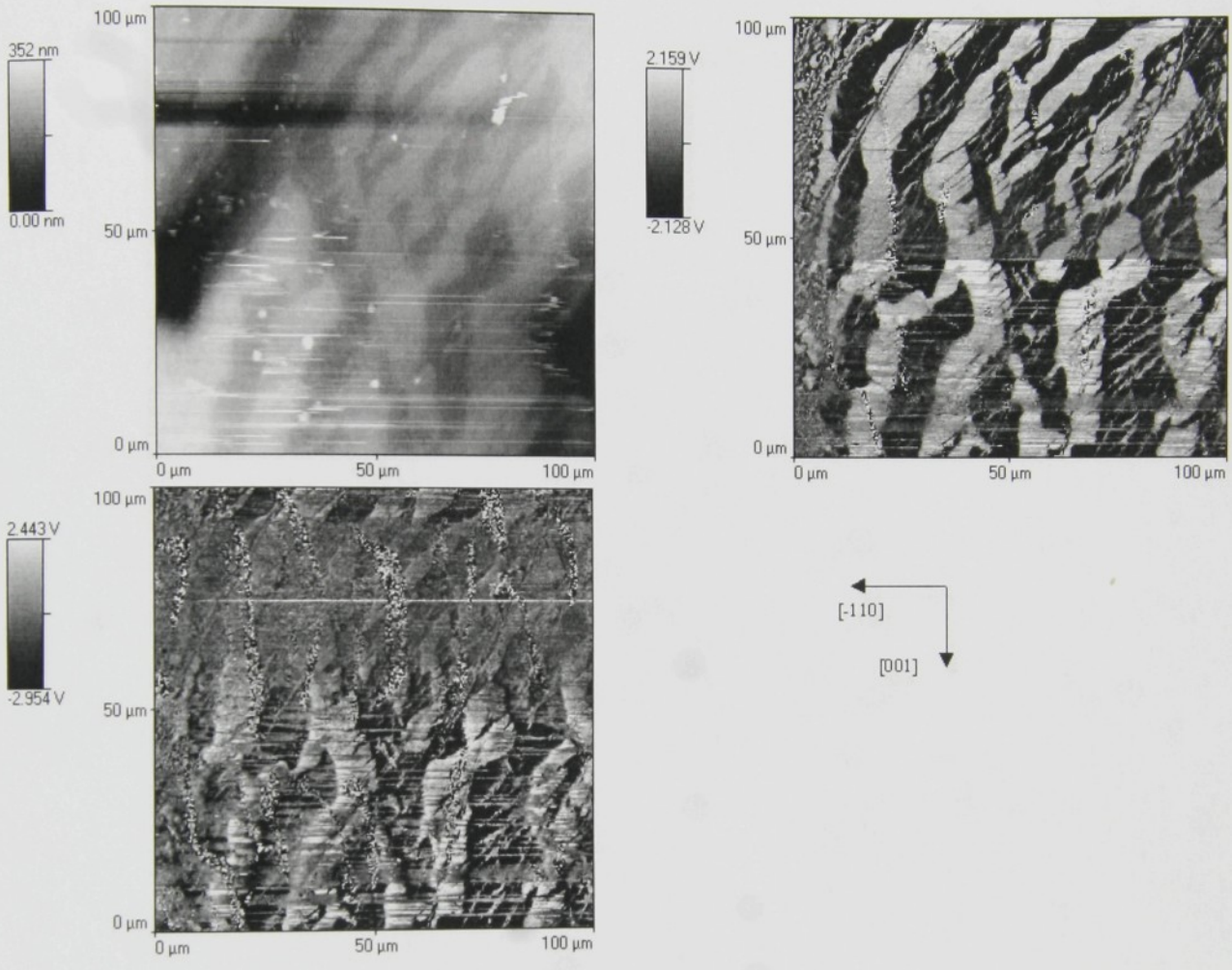

Figure 11. Piezoelectric mode SFM scan on unpoled (110)-oriented PZN-8%PT sample – detail of the upper left corner of the previous image. Topography (upper left), normal (upper right) and in-plane (lower left) piezoelectric response is displayed. The in-plane signal corresponds to $d_{\parallel 2}$.

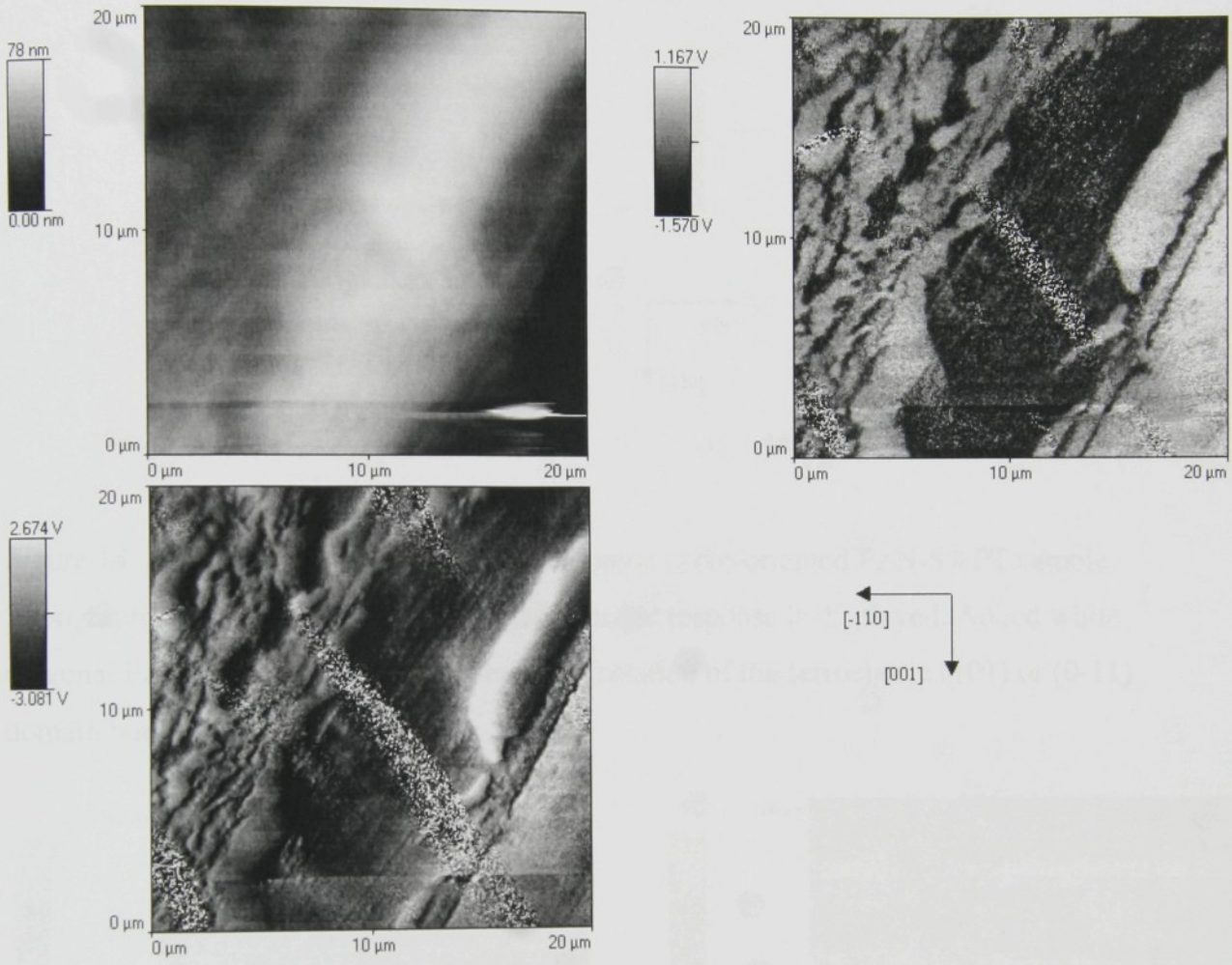

Figure 12. Optical microscopy on unpoled (110)-oriented PZN-8%PT single-crystal (edge = *1 mm*).

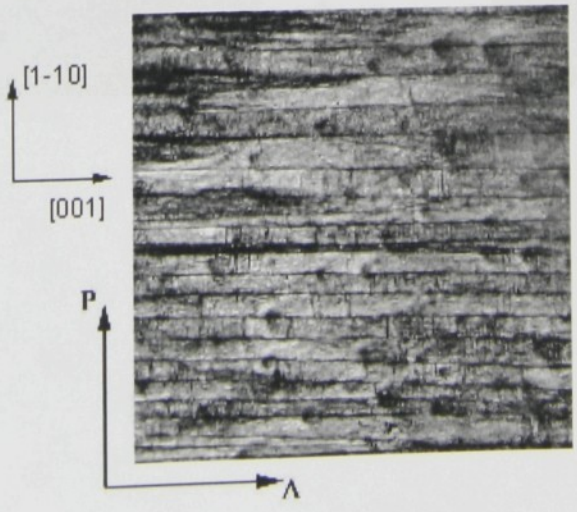

Figure 13. Poling experiment using SFM tip on (110)-surface of unpoled PZN-8%PT crystal. Black region was created during hysteresis loop (+60 V at the end), white region correspond to a -60V pulse applied to the SFM tip. Topography (left) and normal (right) piezoelectric response is displayed.

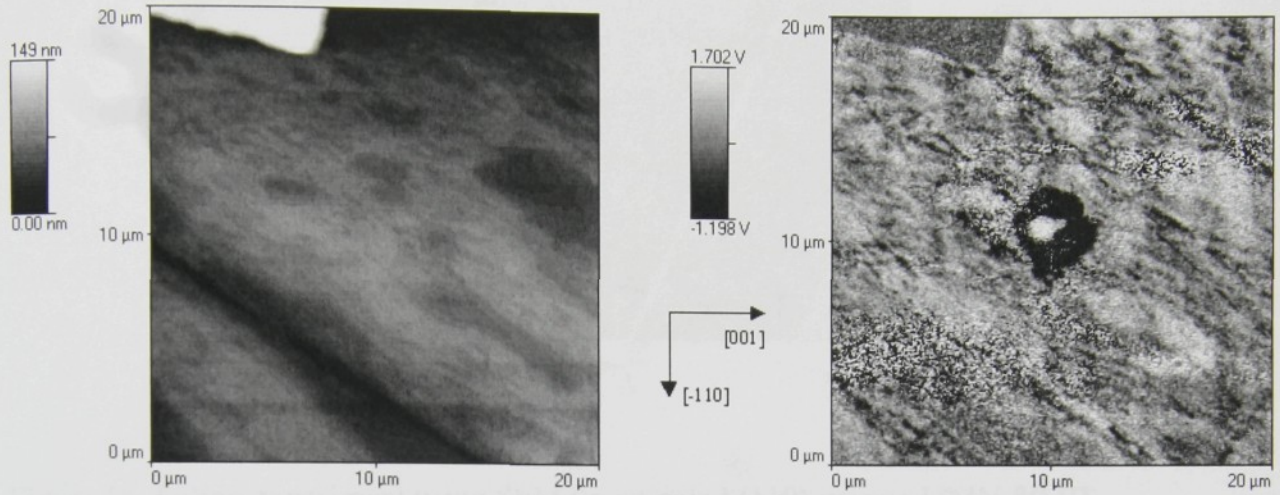

Figure 14. Piezoelectric mode SFM scan on poled (110)-oriented PZN-8%PT sample. Topography (left) and normal (right) piezoelectric response is displayed. Added white diagonal lines correspond to the preferred orientation of the ferroelastic (101) or (0-11) domain walls.

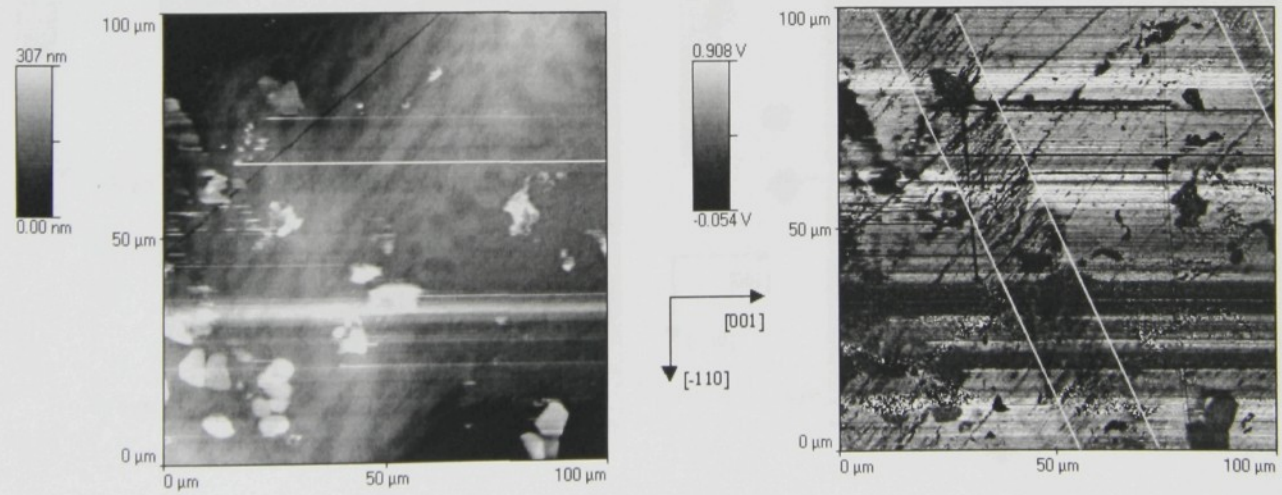

Figure 15. Optical microscopy on poled (110)-oriented PZN-8%PT single-crystal (edge = *1 mm*).

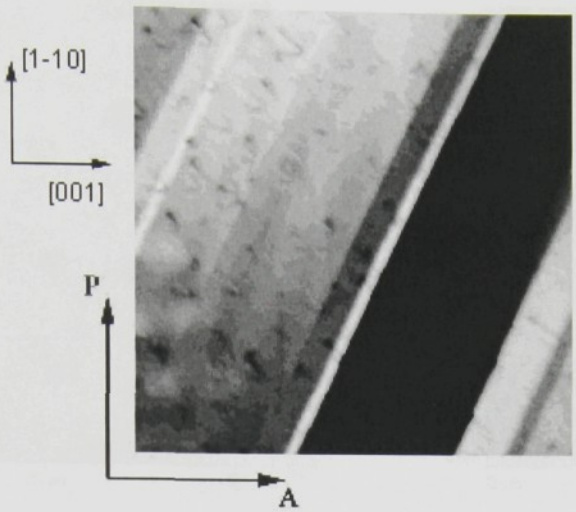

Figure 16. Poling experiment using SFM tip on poled (110)-oriented PZN-8%PT sample. Black and white regions correspond to +30V (top) and -30V (bottom) applied to the SFM tip. Topography (left) and normal (right) piezoelectric response is displayed. Added white rectangles border a region of applied poling voltage.

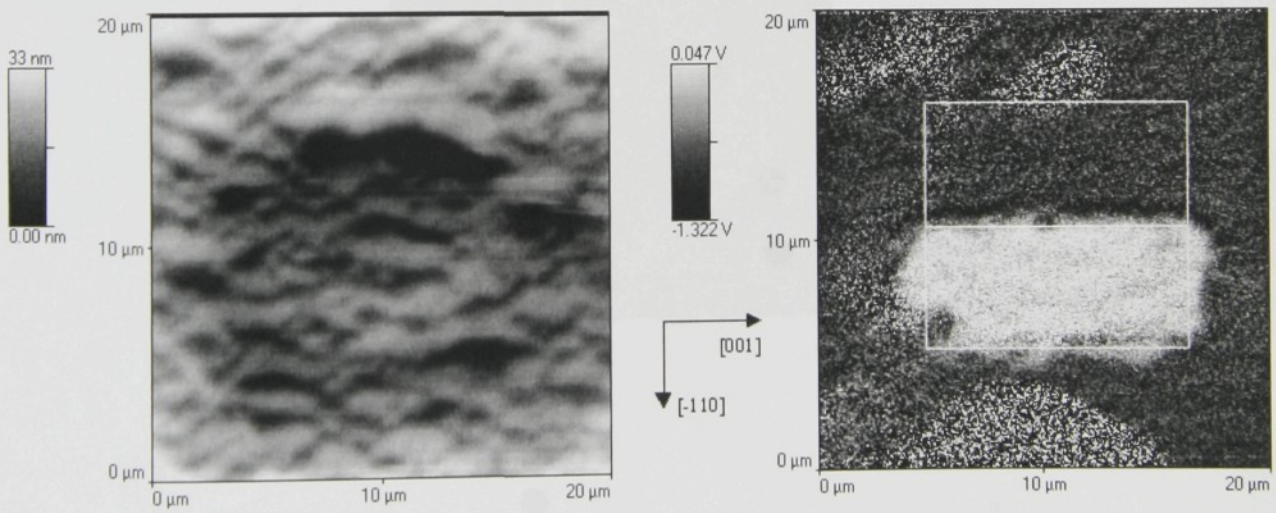

Figure 17. Piezoelectric mode SFM scan on unpoled (110)-oriented PMN-29%PT sample. Topography (left) and normal (right) piezoelectric response is displayed.

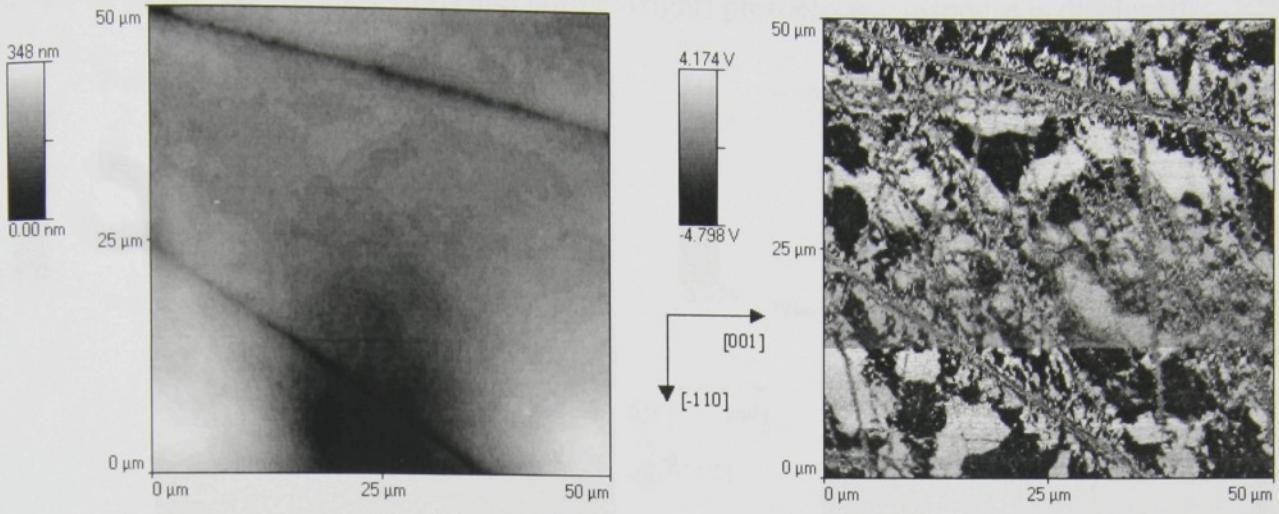

Figure 18. Optical microscopy on unpoled (110)-oriented PMN-29%PT single-crystal (edge=1mm).

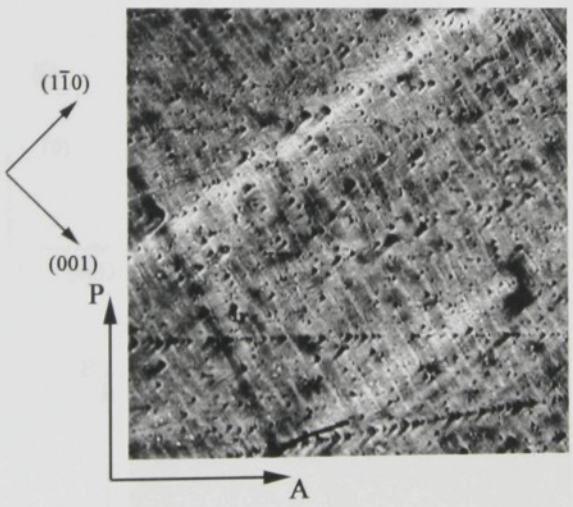

Figure 19. Poling experiment using SFM tip on unpoled (110)-oriented PMN-29%PT sample. Black and white regions correspond to +60V (top) and -60V (bottom) applied to the SFM tip. Topography (left) and normal (right) piezoelectric response is displayed.

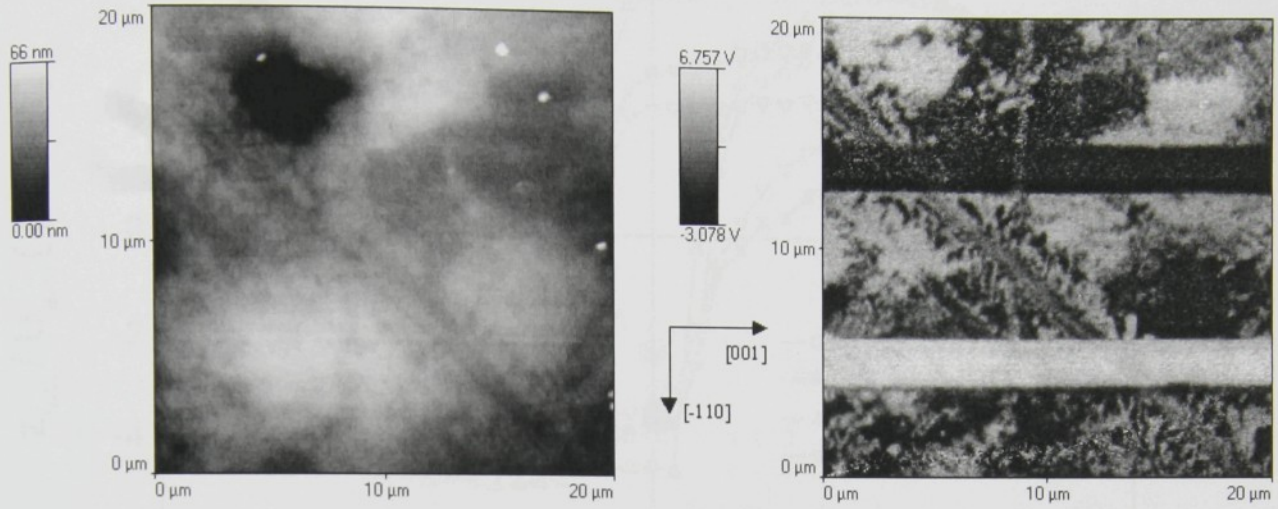

Figure 20. Optical microscopy on poled (110)-oriented PMN-29%PT single-crystal (edge=1mm).

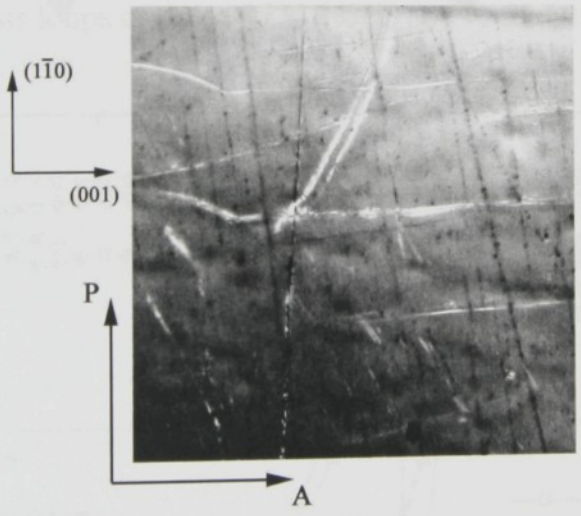

Figure 21. Hysteresis loops of unpoled PZN-8%PT and PMN-29%PT crystals (±60V).

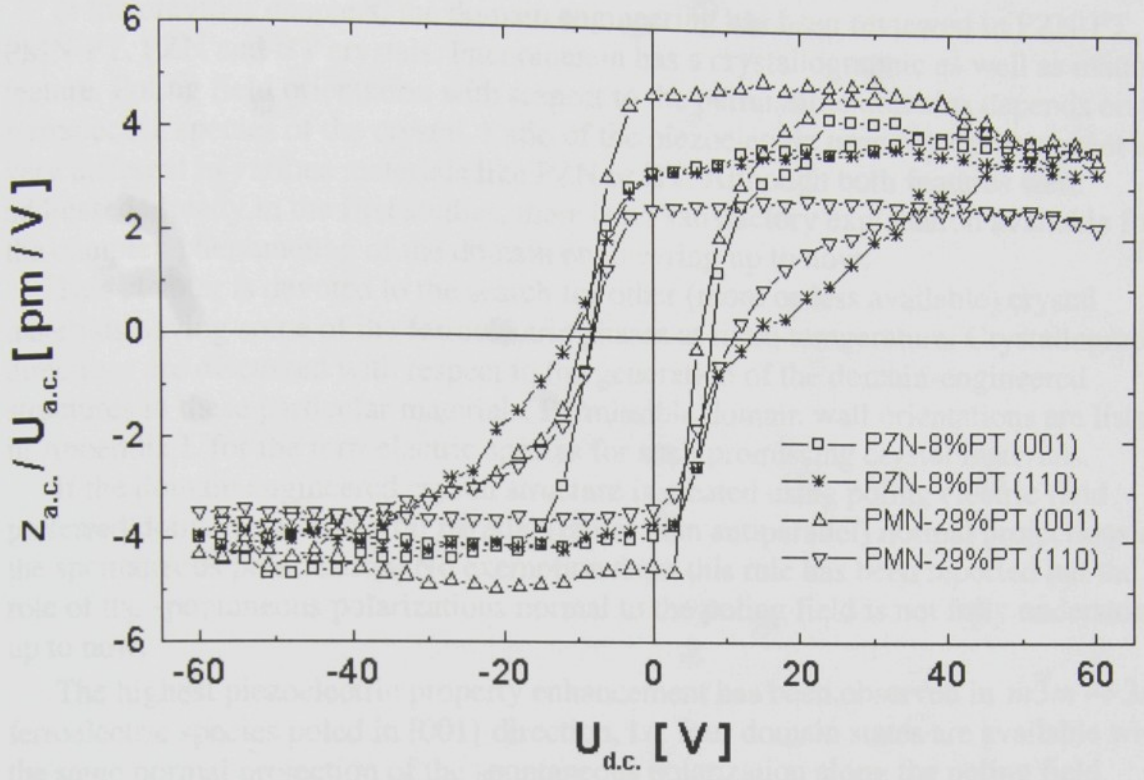

Figure 22. Hysteresis loops of poled PZN-8%PT and PMN-29%PT crystals (±60V).

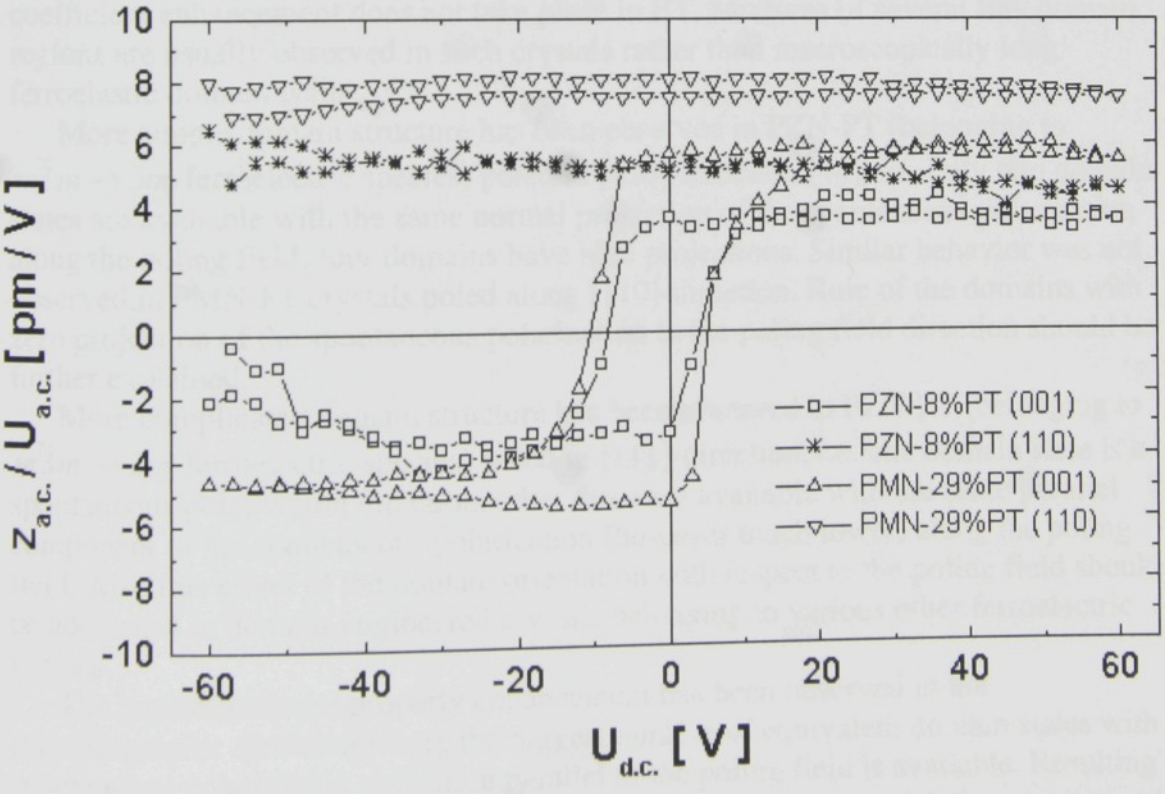

4. Future perspectives of domain engineering in ferroelectric crystals

In the previous chapters, the domain engineering has been reviewed in PZN-PT, PMN-PT, PZN and BT crystals. Phenomenon has a crystallographic as well as material feature. Poling field orientation with respect to the permissible domains depends on the ferroelectric species of the crystal. Ratio of the piezoelectric property enhancement is very different in various materials like PZN or BT. Although both features were addressed already in the first studies, there is no satisfactory explanation available for the complex phenomenon of the domain engineering up to now.

This chapter is devoted to the search for other (more or less available) crystal materials having some of the ferroelectric phases at room temperature. Crystallographic directions are discussed with respect to the generation of the domain-engineered structures in these particular materials. Permissible domain wall orientations are listed in Appendix I. for the ferroelectric species for such promissing crystal materials.

If the domain engineered crystal structure is created using poling electric field preferred domain states exhibit parallel (rather than antiparallel) normal projections of the spontaneous polarization. No exemption from this rule has been reported but the role of the spontaneous polarizations normal to the poling field is not fully understood up to now.

The highest piezoelectric property enhancement has been observed in $m\bar{3}m \rightarrow 3m$ ferroelectric species poled in [001]-direction, i.e. four domain states are available with the same normal projection of the spontaneous polarization along the poling field. Piezoelectric coefficient enhancement is probably further supported by the coexistence of the rhombohedral and tetragonal phases at the morphotropic phase boundary in solid solutions of PZN-PT and PMN-PT (compare material property enhancement in pure PZN crystals and in solid solution of PZN-PT). Similar value of the piezoelectric coefficient enhancement does not take place in BT. Mixtures of several tiny domain regions are usually observed in such crystals rather than macroscopically long ferroelastic domain walls.

More simple domain structure has been observed in PZN-PT (belonging to $m\bar{3}m \rightarrow 3m$ ferroelectric species) poled in [110]-direction [44], i.e. only two domain states are available with the same normal projection of the spontaneous polarization along the poling field, four domains have zero projections. Similar behavior was not observed in PMN-PT crystals poled along [110]-direction. Role of the domains with zero projection of the spontaneous polarization to the poling field direction should be further explained.

More complicated domain structure has been observed in PZN-PT (belonging to $m\bar{3}m \rightarrow 3m$ ferroelectric species) poled in [111]-direction, i.e. one domain state is a spontaneous polarization direction, other three are available with the same parallel component of the spontaneous polarization (however much lower) along the poling field. Also this effect of the domain orientation with respect to the poling field should be addressed in domain-engineered crystals belonging to various other ferroelectric species.

The highest material property enhancement has been observed in the crystallographic direction where the biggest number of equivalent domain states with spontaneous polarization projection parallel to the poling field is available. Resulting domain structure contains mixtures of tiny twin-domain regions of different permissible variants. Consequently, the electromechanical energy of such complicated system is higher than for single-domain crystal state. This is anticipated as a reason for e.g.

hysteresis-free strain induced by the electric field and for better domain wall mobility resulting in superior piezoelectric material coefficients.

Another important question arises about the electric field induced ferroelectric phases in domain-engineered crystal at certain levels of the electric field as reported in PZN-9%PT in [001]-direction [51] and in BT in both [001]- and [111]-directions [25,34]. Open problem is also the question about possible generation of the domain engineered crystals employing also mechanical stresses (or single stress or stress combined with the electric field) on the crystal. Theoretical analysis shows possibility of the creation of even more complicated domain-engineered crystal structures using controlled mechanical stress [1].

Extensive search in Landolt-Börnstein Tables resulted in several crystal materials reported previously to be ferroelectric at room temperature and having more than two domain states:

- perovskites $BaTiO_3$, $PbTiO_3$ ($m\bar{3}m \rightarrow 4mm$), $KNbO_3$ ($m\bar{3}m \rightarrow mm2$), KIO_3 ($3m \rightarrow 1$)
- layer bismuth oxide $Bi_4Ti_3O_{12}$ ($4/mmm \rightarrow m$)
- tungsten bronze $PbNb_2O_6$ ($4/mmm \rightarrow mm2$)
- boracites – $Cu_3B_7O_{13}Br$, $Cu_3B_7O_{13}Cl$, $Fe_3B_7O_{13}Br$, $Fe_3B_7O_{13}I$ ($\bar{4}3m \rightarrow mm2$), $Co_3B_7O_{13}Cl$, $Zn_3B_7O_{13}Cl$, $Fe_3B_7O_{13}Cl$, $Li_4B_7O_{13}Cl$ ($\bar{4}3m \rightarrow 3$ or $\bar{4}3m \rightarrow 3m$)

4.1 Ferroelectric species $m\bar{3}m \rightarrow 4mm$

Possible candidates $BaTiO_3$ (BT), $PbTiO_3$ (PT) belonging to this ferroelectric species are known and extensively studied for a long time. There are six different orientations of the spontaneous polarization vector available for domain engineering [55]. Domain engineering has been partly reported on BT [25,34] already. PT is known as a ferroelectric tetragonal material with relatively high Curie temperature (490°C).

Promissing crystallographic direction of the poling electric field is (Miller indices are listed with respect to the paraelectric cubic phase as marked by the subscript C)

- $[001]_C$ – one spontaneous polarization direction parallel to the poling field, otherwise normal or antiparallel spontaneous polarizations.
- $[110]_C$ – two equivalent spontaneous polarization directions with projections parallel to the poling field, otherwise four normal and two antiparallel spontaneous polarization projections. This poling direction has not been reported yet.
- $[111]_C$ - three equivalent spontaneous polarization directions with projections parallel to the poling field, otherwise three antiparallel spontaneous polarization projections.

BT and PT are also materials with the thermodynamic potentials reported previously [52-54] allowing for the material property calculations. Combining averaging scheme for twin-domain system and thermodynamic theory, e.g. temperature dependence of the effective dielectric constant for twin-domain crystal could be calculated.

4.2 Ferroelectric species $m\bar{3}m \rightarrow mm2$

Possible candidate $KNbO_3$ (KN) belonging to this ferroelectric species are also known and extensively studied in optical applications for a long time. There are twelve different orientations of the spontaneous polarization vector available for domain

engineering [55]. KN undergoes exactly the same sequence of phase transitions as BT, which suggests that the same thermodynamic potential could be used also for this material.

Promissing crystallographic direction of the poling electric field is (Miller indices are listed with respect to the paraelectric cubic phase as marked by the subscript C)

- $[110]_C$ – one spontaneous polarization direction parallel to the poling field, other four equivalent polarization vectors also parallel with different magnitude of the projection, otherwise two normal and four antiparallel spontaneous polarizations projections.
- $[001]_C$ – four equivalent spontaneous polarization directions with projections parallel to the poling field, otherwise four normal and four equivalent antiparallel spontaneous polarization projections.
- $[111]_C$ - three equivalent spontaneous polarization directions with projections parallel to the poling field, otherwise six normal and three equivalent antiparallel spontaneous polarization projections.

New feature of this ferroelectric species is the presence of S-walls (theoretically calculated [45] and observed in KN [46] experimentally) with the orientation dependent on the values of electrostriction coefficients (Appendix I.), i.e. also on the temperature. For comparison see theoretical study on S-wall structure in ferroelastics [57].

4.3 Ferroelectric species $4/mmm \rightarrow m_y$

Possible candidate $Bi_4Ti_3O_{12}$ (BTO) belonging to this ferroelectric species is also known and extensively studied in ferroelectric RAM devices in the form of thin film. There are eight different orientations of the spontaneous polarization vector available for domain engineering [55]. Spontaneous polarization vectors are reported to lie in a-c plane with major component along a-axis in BTO [48].

Promissing crystallographic direction of the poling electric field is (Miller indices are listed with respect to the paraelectric tetragonal phase as marked by the subscript T)

- $[100]_T$ – two and two equivalent spontaneous polarizations with projection (different magnitude) parallel to the poling field, otherwise four polarization vectors with antiparallel spontaneous polarizations projections. The same situation is for $[001]_T$-poling direction.
- $[101]_T$ – similar as above but with different magnitudes of polarization projections
- $[P_x, 0, P_z]_T$ – one spontaneous polarization direction, two other parallel spontaneous polarization directions with different magnitude of the projection to the poling field, two normal polarizations and three antiparallel polarization directions with non-equivalent magnitudes of the projection.

New feature of this ferroelectric species is the presence of S-walls (theoretically calculated [45]) with the orientation dependent on the values of electrostriction coefficients and spontaneous polarization direction (Appendix I.), i.e. also on the temperature.

There is also another variant $4/mmm \rightarrow m_z$ contrary to the ferroelectric species $4/mmm \rightarrow m_y$ discussed above. This species differ in the presence of the permissible pair of perpendicular S-walls, with the orientation dependent also on the electrostriction coefficients and on the polarization direction (Appendix I).

4.4 Ferroelectric species $4/mmm \rightarrow mm2$

There are two non-equivalent species with this symmetry, i.e. $4/mmm \rightarrow m_{\bar{x}y}2_{xy}m_z$ and $4/mmm \rightarrow 2_x m_y m_z$ (Appendix I). While we do not know which species $PbNb_2O_6$ (PNO) belongs to, we will discuss first of them $4/mmm \rightarrow m_{\bar{x}y}2_{xy}m_z$. Second variant of this species is related to the former one by 45°-rotation around $[001]_T$-axis.

There are four different orientations of the spontaneous polarization vector available for domain engineering [55].

Promissing crystallographic direction of the poling electric field is (Miller indices are listed with respect to the paraelectric tetragonal phase as marked by the subscript T)

- $[110]_T$ – one spontaneous polarization is parallel to the poling field, other two are normal and one polarization vector is antiparallel.
- $[100]_T$ or $[010]_T$ – two equivalent spontaneous polarization projections are parallel to the poling field, other two are also equivalent and antiparallel.

Only fixed orientations of the permissible domain walls are allowed for this ferroelectric species (Appendix I).

4.5 Ferroelectric species $\bar{4}3m \rightarrow m_{xy}m_{\bar{x}y}2_z$

Some of the boracite materials exhibit this symmetry of the phase transition. There are six different orientations of the spontaneous polarization vector available for domain engineering [55].

Promissing crystallographic direction of the poling electric field is (Miller indices are listed with respect to the paraelectric cubic phase as marked by the subscript C)

- $[001]_C$ – one spontaneous polarization direction parallel to the poling field, other four equivalent directions are normal and one direction is antiparallel.
- $[110]_C$ – two equivalent spontaneous polarization directions with projections parallel to the poling field, otherwise two normal and two antiparallel spontaneous polarization projections.
- $[111]_C$ or $[-1-1-1]_C$ - three equivalent spontaneous polarization directions with projections parallel to the poling field, otherwise three antiparallel spontaneous polarization projections.

New feature of this ferroelectric species is the presence of S-walls (theoretically calculated [45]) with the orientation dependent on the values of electrostriction coefficients, magnitude of the spontaneous polarization and on the value of piezoelectric coefficient (Appendix I.), i.e. also on the temperature. Another interesting feature is the existence of the pair of domain walls, both neutral (e.g. for P^{II} and P^{V} – see Appendix I). Paraelectric phase is piezoelectric (non-centrosymmetric).

4.6 Ferroelectric species $\bar{4}3m \rightarrow 3_{xyz}m_{\bar{x}y}$

Some of the boracite materials exhibit this symmetry of the phase transition or $\bar{4}3m \rightarrow 3_{xyz}$. Both ferroelectric species exhibit the same domain and domain wall

orientations. There are four different orientations of the spontaneous polarization vector available for domain engineering [55].

Promissing crystallographic direction of the poling electric field is (Miller indices are listed with respect to the paraelectric cubic phase as marked by the subscript C)

- $[111]_C$ – one spontaneous polarization direction parallel to the poling field, other three equivalent directions are antiparallel.
- $[001]_C$ – two equivalent spontaneous polarization directions with projections parallel to the poling field, otherwise two antiparallel spontaneous polarization projections.
- $[110]_C$ - one spontaneous polarization direction with projection parallel to the poling field, one antiparallel and two spontaneous polarizations normal.
- $[-1-1-1]_C$ – three equivalent spontaneous polarization directions parallel to the poling field, one direction antiparallel.

Only fixed orientations of the permissible domain walls are allowed for this ferroelectric species (Appendix I). Paraelectric phase is piezoelectric (non-centrosymmetric).

4.7 Ferroelectric species $3m \rightarrow 1$

This is the most complicated ferroelectric species for our choice of the materials. As already reported [56] no permissible domain wall orientations exist between certain domain states. Both paraelectric and ferroelectric phases belong to polar symmetry, i.e. piezoelectricity is allowed. There are six domain states lying in the plane perpendicular to three-fold axis.

This ferroelectric species allows for the existence of S-walls, whose orientation depend on the electromechanical coefficients (electrostriction coefficients), magnitude and direction of the spontaneous polarization.

While the symmetry is so complicated and we did not get further details about particular material KIO_3 and its domain structure, this species is not further discussed here.

4.8 Conclusions

Several ferroelectric species have been discussed with respect to the promissing directions for the application of poling electric field. Although some crystallographic rules could be applied for the domain and domain wall orientations in general, care must be taken to apply results for particular materials.

In some ferroelectric species S-walls could be present in the domain structures. Their role is not known in domain engineering at all. While S-wall orientation could depend also on the temperature possible new effects could be expected arising during electrical poling at higher temperatures.

Conclusions

Domain engineering is reported in this work as a new promissing method for further piezoelectric material property enhancement applicable in ferroelectric crystals. Due to the random grain orientation this method is not generally useful for similar material property enhancement in ceramic ferroelectrics. Ratio of the piezoelectric coefficient improvement is very different material by material. It seems that the biggest material property improvement takes place in solid solutions of PZN-PT and PMN-PT single crystals, it is somewhat lower in pure crystals of PZN and $BaTiO_3$ (BT).

Detailed overview of the results obtained up to date on domain-engineered crystals of PZN, PZN-PT, PMN-PT and BT is reported. Data are reviewed on domain structure observations, material property coefficient measurements, suggested applications and further phenomena related to the domain-engineered structures.

Theoretical investigations of the effective symmetry of twinned ferroelectric crystal and subsequent effective material property calculations have been done. General method of the material property calculation in two-domain system is presented. For the first time ever reported, right averaging rules are used for all components of the mechanical stress, strain, electric field and displacement. Theoretical analysis is done (including numerical examples) for three most important ferroelectric species $m\bar{3}m \rightarrow 3m$, $m\bar{3}m \rightarrow 4mm$ and $m\bar{3}m \rightarrow mm2$ of the perovskite structures.

Our own domain structure observations by piezoresponse Scanning Force Microscopy (SFM) are presented. Antiparallel domain walls are well visualized using this technique in the unpoled PZN-8%PT and PMN-29%PT crystals what is not possible by the optical polarizing microscopy. On the contrary, it is very rare to visualize ferroelastic domain walls by SFM in poled PZN-8%PT and PMN-29%PT crystals even if they are observed by optical microscopy. Poled crystals of [110]-oriented PZN-8%PT exhibited very stable domain structure in contrast to the same crystal oriented in [001]-direction. Local poling experiments and local hysteresis loops were successfully taken in PZN-8%PT of [001]-orientation and PMN-29%PT crystals of [001]- and [110]-orientation. No re-poling was successful in [110]-oriented cut of PZN-8%PT crystal at the electric field used.

Further perspectives in domain engineering are discussed. An extensive search for other crystal candidates for domain-engineered structures has been performed in the last part of this work. Electric field directions applicable for creation of the domain-engineered structure are specified for certain ferroelectric species corresponding to the symmetry of new possible candidates.

Further research on the domain engineering must include an attempt for measurement or calculation of the single-domain material properties of domain-engineered PZN-PT and PMN-PT crystals (such data are not available today). Also the origin of the extremely large values of piezoelectric coefficients in domain-engineered crystals should be explained. Role of the morphotropic phase boundary in solid solution of PZN-PT and PMN-PT, crystallographic as well as material feature of the material property enhancement must be solved before these materials come into everyday use in the technical applications.

Domain engineering could serve as a new tool for designing "smart" ferroelectric materials for various technical applications in the future. The main idea of the engineering of the domain structure is basically applicable also in other types of ferroic materials. Along with the search for new materials, combination of phases in composite materials etc., domain engineering is new promissing method for getting desired material property in ferroelectric materials.

Appendix I

Permissible domain wall orientations in $m\bar{3}m \rightarrow 3m$ ferroelectrics [45]

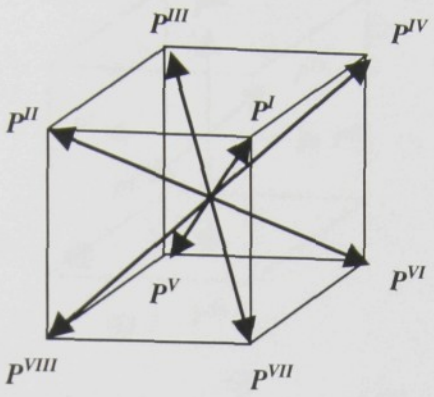

$$P^{I} = \frac{1}{\sqrt{3}} P_S(111),\ P^{II} = \frac{1}{\sqrt{3}} P_S(1\,\bar{1}\,1),\ P^{III} = \frac{1}{\sqrt{3}} P_S(\bar{1}\,\bar{1}\,1),\ P^{IV} = \frac{1}{\sqrt{3}} P_S(\bar{1}\,11),$$

$$P^{V} = \frac{1}{\sqrt{3}} P_S(\bar{1}\,\bar{1}\,\bar{1}),\ P^{VI} = \frac{1}{\sqrt{3}} P_S(\bar{1}\,1\,\bar{1}),\ P^{VII} = \frac{1}{\sqrt{3}} P_S(11\,\bar{1}),\ P^{VIII} = \frac{1}{\sqrt{3}} P_S(1\,\bar{1}\,\bar{1})$$

Table I.1. Permissible domain wall orientations in $m\bar{3}m \rightarrow 3m$ ferroelectrics

	P^{I}	P^{II}	P^{III}	P^{IV}	P^{V}	P^{VI}	P^{VII}	P^{VIII}
P^{I}	N/A	(010) (101)	(001) (110)	(100) (011)	any	(010) (101)	(001) (110)	(100) (011)
P^{II}		N/A	(100) (0-11)	(001) (-110)	(010) (101)	any	(100) (0-11)	(001) (-110)
P^{III}			N/A	(010) (-101)	(001) (110)	(100) (0-11)	any	(010) (-101)
P^{IV}				N/A	(100) (011)	(001) (-110)	(010) (-101)	any
P^{V}					N/A	(010) (101)	(001) (110)	(100) (011)
P^{VI}						N/A	(100) (0-11)	(001) (-110)
P^{VII}							N/A	(010) (-101)
P^{VIII}								N/A

Permissible domain wall orientations in $m\bar{3}m \rightarrow 4mm$ ferroelectrics [45]

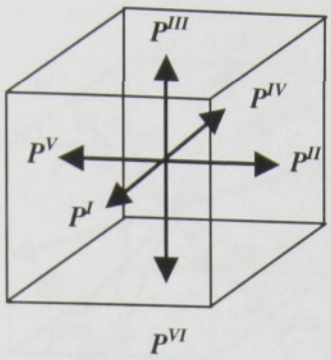

$P^{I} = P_S(100)$, $P^{II} = P_S(010)$, $P^{III} = P_S(001)$,
$P^{IV} = P_S(\bar{1}00)$, $P^{V} = P_S(0\bar{1}0)$, $P^{VI} = P_S(00\bar{1})$

Table I.2. Permissible domain wall orientations in $m\bar{3}m \rightarrow 4mm$ ferroelectrics

	P^{I}	P^{II}	P^{III}	P^{IV}	P^{V}	P^{VI}
P^{I}	N/A	(110) (1-10)	(101) (10-1)	any	(110) (1-10)	(101) (10-1)
P^{II}		N/A	(011) (01-1)	(110) (1-10)	any	(011) (01-1)
P^{III}			N/A	(101) (10-1)	(011) (01-1)	any
P^{IV}				N/A	(110) (1-10)	(101) (10-1)
P^{V}					N/A	(011) (01-1)
P^{VI}						N/A

Permissible domain wall orientations in $m\bar{3}m \rightarrow mm2$ ferroelectrics [45]

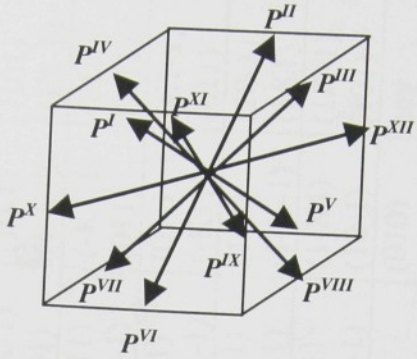

$$P^{I} = \frac{1}{\sqrt{2}} P_S(101),\ P^{II} = \frac{1}{\sqrt{2}} P_S(\bar{1}01),\ P^{III} = \frac{1}{\sqrt{2}} P_S(011),\ P^{IV} = \frac{1}{\sqrt{2}} P_S(0\bar{1}1)$$

$$P^{V} = \frac{1}{\sqrt{2}} P_S(\bar{1}0\bar{1}),\ P^{VI} = \frac{1}{\sqrt{2}} P_S(10\bar{1}),\ P^{VII} = \frac{1}{\sqrt{2}} P_S(0\bar{1}\,\bar{1}),\ P^{VIII} = \frac{1}{\sqrt{2}} P_S(01\bar{1})$$

$$P^{IX} = \frac{1}{\sqrt{2}} P_S(110),\ P^{X} = \frac{1}{\sqrt{2}} P_S(1\bar{1}0),\ P^{XI} = \frac{1}{\sqrt{2}} P_S(\bar{1}\,\bar{1}0),\ P^{XII} = \frac{1}{\sqrt{2}} P_S(\bar{1}10)$$

$$K = \frac{Q_{44}}{Q_{11} - Q_{12}}$$

Table I.3. Permissible domain wall orientations in $m\bar{3}m \rightarrow mm2$ ferroelectrics

	P^{I}	P^{II}	P^{III}	P^{IV}	P^{V}	P^{VI}	P^{VII}	P^{VIII}	P^{IX}	P^{X}	P^{XI}	P^{XII}
P^{I}	N/A	(100) (001)	(1-10) (11K)	(110) (1-1K)	any	(001) (100)	(11K) (1-10)	(1-1K) (110)	(01-1) (K11)	(011) (-K1-1)	(K11) (01-1)	(-K1-1) (011)
P^{II}		N/A	(110) (1-1-K)	(1-10) (11-K)	(001) (100)	any	(1-1-K) (110)	(11-K) (1-10)	(K1-1) (011)	(-K11) (01-1)	(011) (K1-1)	(01-1) (-K11)
P^{III}			N/A	(010) (001)	(11K) (1-10)	(1-1-K) (110)	any	(001) (010)	(10-1) (1K1)	(1-K-1) (101)	(1K1) (10-1)	(101) (1-K-1)
P^{IV}				N/A	(1-1K) (110)	(11-K) (1-10)	(001) (010)	any	(1K-1) (101)	(10-1) (1-K1)	(101) (1K-1)	(1-K1) (10-1)
P^{V}					N/A	(100) (001)	(1-10) (11K)	(110) (1-1K)	(K11) (01-1)	(-K1-1) (011)	(01-1) (K11)	(011) (-K1-1)
P^{VI}						N/A	(110) (1-1-K)	(1-10) (11-K)	(011) (K1-1)	(01-1) (-K11)	(K1-1) (011)	(-K11) (01-1)
P^{VII}							N/A	(010) (001)	(1K1) (10-1)	(101) (1-K-1)	(10-1) (1K1)	(1-K-1) (101)
P^{VIII}								N/A	(101) (1K-1)	(1-K1) (10-1)	(1K-1) (101)	(10-1) (1-K1)
P^{IX}									N/A	(010) (100)	any	(100) (010)
P^{X}										N/A	(100) (010)	any
P^{XI}											N/A	(010) (100)
P^{XII}												N/A

Permissible domain wall orientations in $\bar{4}3m \rightarrow m_{xy}m_{\bar{x}y}2_z$ ferroelectrics [45]

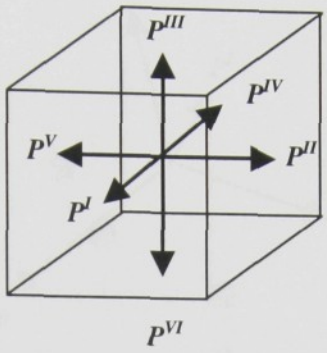

$P^I = P_S(100)$, $P^{II} = P_S(010)$, $P^{III} = P_S(001)$,
$P^{IV} = P_S(\bar{1}00)$, $P^V = P_S(0\bar{1}0)$, $P^{VI} = P_S(00\bar{1})$

$$K = \frac{b_{14}}{P_S(Q_{11} - Q_{12})}$$

Table I.4. Permissible domain wall orientations in $\bar{4}3m \rightarrow m_{xy}m_{\bar{x}y}2_z$ ferroelectrics

	P^I	P^{II}	P^{III}	P^{IV}	P^V	P^{VI}
P^I	N/A	(-110) (11-K)	(-101) (1-K1)	(010) (001)	(110) (-11-K)	(101) (-1-K1)
P^{II}		N/A	(0-11) (-K11)	(110) (1-1-K)	(100) (001)	(011) (-K-11)
P^{III}			N/A	(101) (1-K-1)	(011) (-K1-1)	(100) (010)
P^{IV}				N/A	(-110) (11K)	(-101) (1K1)
P^V					N/A	(0-11) (K11)
P^{VI}						N/A

Permissible domain wall orientations in $\bar{4}3m \rightarrow 3_{xyz} m_{\bar{x}y}$ ferroelectrics [45]

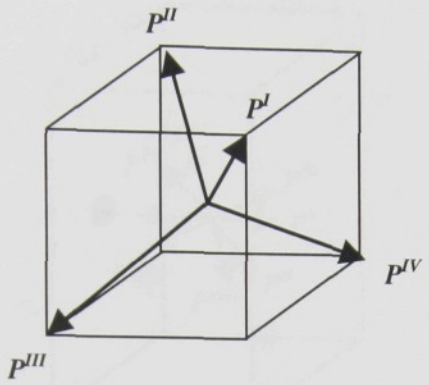

$$P^{I} = \frac{1}{\sqrt{3}} P_S(111),\ P^{II} = \frac{1}{\sqrt{3}} P_S(\bar{1}\,\bar{1}\,1),\ P^{III} = \frac{1}{\sqrt{3}} P_S(1\,\bar{1}\,\bar{1}),\ P^{IV} = \frac{1}{\sqrt{3}} P_S(\bar{1}\,1\,\bar{1})$$

Table I.5. Permissible domain wall orientations in $\bar{4}3m \rightarrow 3_{xyz} m_{\bar{x}y}$ ferroelectrics

	P^{I}	P^{II}	P^{III}	P^{IV}
P^{I}	N/A	(001) (110)	(100) (011)	(010) (101)
P^{II}		N/A	(010) (-101)	(100) (0-11)
P^{III}			N/A	(001) (1-10)
P^{IV}				N/A

Permissible domain wall orientations in $4/mmm \rightarrow m_y$ ferroelectrics [45]

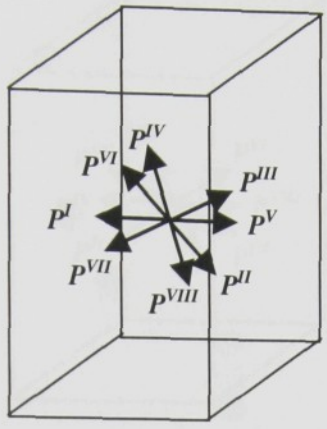

$$P^{I} = (P_x, 0, P_z),\ P^{II} = (0, P_x, P_z),\ P^{III} = (-P_x, 0, P_z),\ P^{IV} = (0, -P_x, P_z)$$
$$P^{V} = (-P_x, 0, -P_z),\ P^{VI} = (0, -P_x, -P_z),\ P^{VII} = (P_x, 0, -P_z),\ P^{VIII} = (0, P_x, -P_z)$$
$$K = \frac{Q_{44}}{Q_{11} - Q_{12}} \frac{P_z}{P_x}$$

Table I.6. Permissible domain wall orientations in $4/mmm \rightarrow m_y$ ferroelectrics

	P^{I}	P^{II}	P^{III}	P^{IV}	P^{V}	P^{VI}	P^{VII}	P^{VIII}
P^{I}	N/A	(-110) (11K)	(100) (001)	(110) (-11-K)	any	(11K) (-110)	(001) (100)	(-11-K) (110)
P^{II}		N/A	(110) (1-1K)	(010) (001)	(11K) (-110)	any	(1-1-K) (110)	(001) (010)
P^{III}			N/A	(1-10) (11-K)	(001) (100)	(1-1-K) (110)	any	(11-K) (1-10)
P^{IV}				N/A	(-11-K) (110)	(001) (010)	(11-K) (1-10)	any
P^{V}					N/A	(-110) (11K)	(100) (001)	(110) (-11-K)
P^{VI}						N/A	(110) (1-1-K)	(010) (001)
P^{VII}							N/A	(1-10) (11-K)
P^{VIII}								N/A

Permissible domain wall orientations in $4/mmm \rightarrow m_z$ ferroelectrics [45]

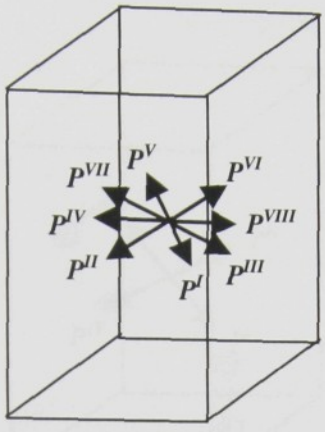

$$P^{I} = (P_x, P_y, 0),\ P^{II} = (P_x, -P_y, 0),\ P^{III} = (P_y, P_x, 0),\ P^{IV} = (P_y, -P_x, 0)$$

$$P^{V} = (-P_x, -P_y, 0),\ P^{VI} = (-P_x, P_y, 0),\ P^{VII} = (-P_y, -P_x, 0),\ P^{VIII} = (-P_y, P_x, 0)$$

$$K = \frac{Q_{66}}{Q_{11} - Q_{12}} \frac{P_x P_y}{P_y^2 - P_x^2}$$

$$L^{+} = -K + \sqrt{K^2 + 1}$$

$$L^{-} = -K - \sqrt{K^2 + 1}$$

Table I.7. Permissible domain wall orientations in $4/mmm \rightarrow m_z$ ferroelectrics

	P^{I}	P^{II}	P^{III}	P^{IV}	P^{V}	P^{VI}	P^{VII}	P^{VIII}
P^{I}	N/A	(010) (100)	(1-10) (110)	(1L^{+}0) (1L^{-}0)	any	(100) (010)	(110) (1-10)	(1L^{-}0) (1L^{+}0)
P^{II}		N/A	(1-10) (110)	(110) (1-10)	(100) (010)	any	(110) (1-10)	(1-10) (110)
P^{III}			N/A	(100) (010)	(110) (1-10)	(110) (1-10)	any	(010) (100)
P^{IV}				N/A	(1L^{-}0) (1L^{+}0)	(1-10) (110)	(010) (100)	any
P^{V}					N/A	(010) (100)	(1-10) (110)	(1L^{+}0) (1L^{-}0)
P^{VI}						N/A	(1-10) (110)	(110) (1-10)
P^{VII}							N/A	(100) (010)
P^{VIII}								N/A

Permissible domain wall orientations in $4/mmm \rightarrow m_{\bar{x}y}2_{xy}m_z$ ferroelectrics [45]

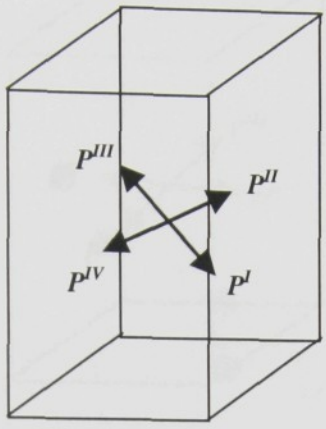

$$P^{I} = \frac{1}{\sqrt{2}} P_S(110),\ P^{II} = \frac{1}{\sqrt{2}} P_S(\bar{1}10),\ P^{III} = \frac{1}{\sqrt{2}} P_S(\bar{1}\bar{1}0),\ P^{IV} = \frac{1}{\sqrt{2}} P_S(1\bar{1}0)$$

Table I.8. Permissible domain wall orientations in $4/mmm \rightarrow m_{\bar{x}y}2_{xy}m_z$ ferroelectrics

	P^{I}	P^{II}	P^{III}	P^{IV}
P^{I}	N/A	(100) (010)	any	(010) (100)
P^{II}		N/A	(010) (100)	any
P^{III}			N/A	(100) (010)
P^{IV}				N/A

Permissible domain wall orientations in $4/mmm \rightarrow 2_x m_y m_z$ ferroelectrics [45]

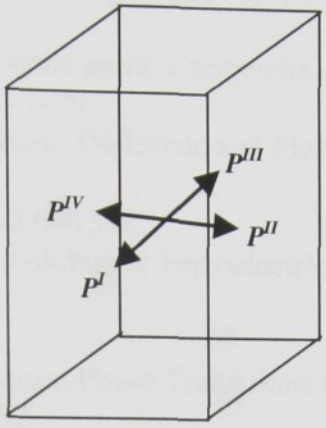

$P^I = P_S(100),\ P^{II} = P_S(010),\ P^{III} = P_S(\bar{1}00),\ P^{IV} = P_S(0\bar{1}0)$

Table I.9. Permissible domain wall orientations in $4/mmm \rightarrow 2_x m_y m_z$ ferroelectrics

	P^I	P^{II}	P^{III}	P^{IV}
P^I	N/A	(110) (1-10)	any	(110) (1-10)
P^{II}		N/A	(110) (1-10)	any
P^{III}			N/A	(110) (1-10)
P^{IV}				N/A

Bibliography

[1] J.Fousek, D.B.Litvin, L.E.Cross: Domain Geometry Engineering and Domain Average Engineering in Ferroics
J.Phys.Condens.Matter **13** (2001) L33-L38
[2] R.E.Newnham: Composite Electroceramics
Ferroelectrics **68** (1986) 1-32
[3] A.Safari: Development of Piezoelectric Composites for Transducers
J.Phys.III France **4** (1994) 1129-1149
[4] J.Kuwata, K.Uchino, S.Nomura: Dielectric and Piezoelectric Properties of 0.91PZN-0.09PT Single Crystals
Jpn.J.Appl.Phys. **21**, 9 (1982) 1298-1302
[5] S.Nomura, T.Takahashi, Y.Yokomizo: Ferroelectric Properties in the System PZN-PT
J.Phys.Soc.Jpn. **27** (1969) 262
[6] J.Kuwata, K.Uchino, S.Nomura: Phase Transitions in the PZN-PT System
Ferroelectrics **37** (1981) 579-582
[7] T.R.Shrout, J.Fielding: Relaxor Ferroelectric Materials
Ultrasonic Symposium (1990) 711-720
[8] S.E.Park, T.R.Shrout: Ultrahigh Strain and Piezoelectric Behavior in Relaxor Based Ferroelectric Single Crystals
J.Appl.Phys. **82**, 4 (1997) 1804-1811
[9] S.E.Park, T.R.Shrout: Characteristics of Relaxor-Based Piezoelectric Single Crystals for Ultrasonic Transducers
IEEE Trans UFFC **44**, 5 (1997) 1140-1147
[10] M.L.Mulvihill, S.E.Park, G.Risch, Z.Li, K.Uchino: The Role of Processing Variables in the Flux Growth of Lead Zinc Niobate-Lead Titanate Ferroelectric Single Crystals
Jpn.J.Appl.Phys. **35**, 7 (1996) 3984-3990
[11] S.Shimanuki, S.Saito, Y.Yamashita: Single Crystal of the PZN-PT System Grown by the Vertical Bridgeman Method and Its Characterization
Jpn.J.Appl.Phys. **37**, 6A (1998) 3382-3385
[12] U.Belegundu, X.H.Du, L.E.Cross, K.Uchino: In Situ Observation of Domains in 0.91PZN-0.09PT Single Crystals
Ferroelectrics **221** (1999) 67-71
[13] S.Wada, S.E.Park, L.E.Cross, T.R.Shrout: Engineered Domain Configuration in Rhombohedral PZN-PT Single Crystals and their Ferroelectric Related Properties
Ferroelectrics **221** (1999) 147-155
[14] S.Wada, S.E.Park, L.E.Cross, T.R.Shrout: Domain Configuration and Ferroelectric Related Properties of Relaxor Based Single Crystals
J.Korean Physical Soc. **32** (1998) S1290-S1293
[15] J.Yin, W.Cao: Domain Configurations in Domain Engineered 0.955PZN-0.045PT Single Crystals
J.Appl.Phys. **87**,10 (2000) 7438-7441
[16] K.Fujishiro, R.Vlokh, Y.Uesu, Y.Yamada, J.M.Kiat, B.Dkhil, Y.Yamashita: Optical Observation of Heterophase and Domain Structures in Relaxor Ferroelectrics PZN-9%PT
Jpn.J.Appl.Phys. **37**, 9B (1998) 5246-5248
[17] Z.G.Ye, M.Dong, L.Zhang: Domain Structures and Phase Transitions of the Relaxor-based Piezo/Ferroelectric (1-x)PZN-xPT Single Crystals

Ferroelectrics **229** (1999) 223-232
[18] N.Setter, L.E.Cross: An Optical Study of the Ferroelectric Relaxors PMN, PST, PSN
Ferroelectrics **37** (1981) 551-554
[19] Z.G.Ye, M.Dong: Morphotropic Domain Structures and Phase Transitions in Relaxor-based Piezo/Ferroelectric (1-x)PMN-xPT Single Crystals
J.Appl.Phys. **87**, 5 (2000) 2312-2319
[20] Z.W.Yin, H.S.Luo, P.Ch.Wang, G.S.Xu: Growth, Characterization and Properties of Relaxor Ferroelectric PMN-PT Single Crystals
Ferroelectrics **229** (1999) 207-216
[21] M.L.Mulvihill, L.E.Cross, K.Uchino: Low-Temperature Observation of Relaxor Ferroelectric Domains in Lead Zinc Niobate
J.Amer.Ceram.Soc. **78**, 12 (1995) 3345-3351
[22] S.Wada, S.E.Park, L.E.Cross, T.R.Shrout: Defect-induced Domain Configuration in Relaxor PZN Single Crystal and Its Origin
Trans.Mater.Res.Soc.Japan **24**, 1 (1999) 19-22
[23] Morgan Matroc Ltd., *Data Book on PZT ceramics*
[24] H.Yu, C.A.Randall: Dendritic Domain Configurations in PZN-PT Single Crystals
J.Appl.Phys. **86**, 10 (1999) 5733-5738
[25] S.Wada, S.Suzuki, T.Noma, T.Suzuki, M. Osada, M.Kakihana, S.E.Park, L.E.Cross, T.R.Shrout: Enhanced Piezoelectric Property of Barium Titanate Single Crystals with Engineered Domain Configurations
Jpn.J.Appl.Phys. **38**, 9B (1999) 5505-5511
[26] J.Yin, B.Jiang, W.Cao: Elastic, Piezoelectric and Dielectric Properties of 0.955PZN-0.045PT Single Crystal with Designed Multidomains
IEEE Trans UFFC **47**, 1 (2000) 285-291
[27] D.S.Paik, S.E.Park, T.R.Shrout, W.Hackenberger: Dielectric and Piezoelectric Properties of Perovskite Materials at Cryogenic Temperatures
J.Mater.Sci. **34** (1999) 469-473
[28] S.Nomura, H.Arima, F.Kojima: Quadratic Electro-Optic Effect in the System PZN-PT
Jpn.J.Appl.Phys. **12**, 4 (1973) 531-535
[29] G.Robert, D.Damjanovic, N.Setter: Temperature Dependence of Piezoelectric Properties for Relaxor-Ferroelectric Solid Solutions Undergoing a Rhombohedral to Tetragonal Phase Transition
Ferroelectrics **224** (1999) 97-104
[30] K.Takemura, M.Ozgul, V.Bornand, S.Trolier-McKinstry, C.A.Randall: Fatigue Anisotropy in Single Crystal PZN-PT
J.Appl.Phys. **88**, 12 (2000) 7272-7277
[31] H.Yu, V.Gopalan, J.Sindel, C.A.Randall: Domain Switching and Electromechanical Properties of Pulse Poled PZN-PT Crystals
J.Appl.Phys. **89**, 1 (2001) 561-567
[32] A.A.Bokov, Z.G.Ye: Freezing of Dipole Dynamics in Relaxor Ferroelectric PMN-PT as Evidenced by Dielectric Spectroscopy
J.Phys.:Condens.Matter **12** (2000) L541-L548
[33] D.Viehland, J.Powers: Effect of Uniaxial Stress on the Electromechanical Properties of 0.7PMN-0.3PT Crystals and Ceramics
J.Appl.Phys. **89**, 3 (2001) 1820-1825
[34] S.E.Park, S.Wada, L.E.Cross, T.R.Shrout: Crystallographically Engineered $BaTiO_3$ Single Crystals for High-performance Piezoelectrics

J.Appl.Phys. **86**, 5 (1999) 2746-2750
[35] K.Abe, O.Furukawa, H.Imagawa: Calculations Concerning the Phase Diagram, Dielectric Constant and Lattice Parameters for the PZN-PT Solid Solution
Ferroelectrics **87** (1988) 55-64
[36] J.Erhart, W.Cao: Effective Material Properties in Twinned Ferroelectric Crystals
J.Appl.Phys. **86**, 2 (1999) 1073-1081
[37] J.Erhart, W.Cao: Effective Symmetry and Physical Properties of Twinned Perovskite Ferroelectric Single Crystals
J.Mater.Research **16**, 2 (2001) 570- 578
[38] S.Saitoh, T.Kobayashi, K.Harada, S.Shimanuki, Y.Yamashita: A 20MHz Single-Element Ultrasonic Probe Using 0.91PZN-0.09PT Single Crystal
IEEE Trans. UFFC **45**, 4 (1998) 1071-1076
[39] S.Saitoh, T.Kobayashi, K.Harada, S.Shimanuki, Y.Yamashita: Forty-Channel Phased Array Ultrasonic Probe Using 0.91PZN-0.09PT Single Crystal
IEEE Trans. UFFC **46**, 1 (1999) 152-157
[40] S.W.Choi, T.R.Shrout, S.J.Jang, A.S.Bhalla: Dielectric and Pyroelectric Properties in the PMN-PT System
Ferroelectrics **100** (1989) 29-38
[41] S.E.Park, T.R.Shrout, P.Bridenbaugh, J.Rottenberg, G.M.Loiacono: Electric Field Induced Anisotropy in Electrostrictive PMN-PT Crystals
Ferroelectrics **207** (1998) 519-526
[42] T.R.Shrout, Z.P.Chang, N.Kim, S.Markgraf: Dielectric Behavior of Single Crystals near the PMN-PT Morphotropic Phase Boundary
Ferroelectrics Letters **12** (1990) 63-69
[43] M.Abplanalp, D.Barošová, P.Bridenbaugh, J.Erhart, J.Fousek, P.Günter, J.Nosek, M.Šulc: Ferroelectric Domain Structures in PZN-8%PT Single Crystals Studied by Scanning Force Microscopy
Solid State Communications (accepted)
[44] M.Abplanalp, D.Barošová, P.Bridenbaugh, J.Erhart, J.Fousek, P.Günter, J.Nosek, M.Šulc: Ferroelectric Domain Structures in PZN-8%PT and PMN-29%PT Single Crystals Studied by Scanning Force Microscopy
J.Appl.Phys. (submitted)
[45] J.Fousek, V.Janovec: The Orientation of Domain Walls in Twinned Ferroelectric Crystals
J. Appl. Phys. **40** (1969) 135-142
[46] E.Wiesendanger: Domain Structures in Orthorhombic $KNbO_3$ and Characterization of Single Domain Crystals
Czech.J.Phys. **B23** (1973) 91-99
[47] E.Aksakaya, G.W.Farnell: Effective Elastic and Piezoelectric Constants of Superlattices
J.Appl.Phys. **64** (1988) 4469-4473
[48] *Landolt-Börnstein Tables*, Springer Verlag, Berlin 1969
Group III Vols.3,9,16
[49] J.F.Nye: *Physical Properties of Crystals*
Clarendon, Oxford, 1957
[50] M.Zgonik, R.Schlesser, I.Biaggio, P.Günter: Electro- and Acousto-optic Properties of $KNbO_3$ Crystals
Ferroelectrics **158** (1994) 217-222
[51] S.F.Liu, S.E.Park, T.R.Shrout, L.E.Cross: Electric Field Dependence of Piezoelectric Properties for Rhombohedral 0.955PZN-0.045PT Single Crystals

J.Appl.Phys. **85**, 5 (1999) 2810-2814
[52] A.F.Devonshire: Theory of Barium Titanate I
Phil.Mag. **40**, Serie 7, 309 (1949) 1040-1063
[53] A.F.Devonshire: Theory of Barium Titanate II
Phil.Mag. **42**, Serie 7, 333 (1951) 1065-1079
[54] M.J.Haun, E.Furman, S.J.Jang, H.A.McKinstry, L.E.Cross: Thermodynamic theory of $PbTiO_3$
J.Appl.Phys. **62**, 8 (1987) 3331-3338
[55] V.Janovec, V.Dvořák, J.Petzelt: Symmetry Classification and Properties of Equitranslational Structural Phase Transitions
Czech.J.Phys. **B25** (1975) 1362-1396
[56] J.Fousek: Permissible Domain Walls in Ferroelectric Species
Czech.J.Phys. **B21** (1971) 955-968
[57] J.Erhart, W.Cao, J.Fousek: The Structure of S-domain Walls in $m\bar{3}m \rightarrow mmm$ Ferroelastics
Ferroelectrics (accepted)